SUPPLEMENTARY METHODS

Biochemical assays. Serum alanine aminotransferase (ALT), alkaline phosphatase (ALP), and total bilirubin (TBIL) levels were determined using a Catalyst Dx Chemistry Analyzer (IDEXX Laboratories, Westbrook, ME). Tissue bile acid concentration was evaluated using the Total Bile Acid Assays and following manufacturer's instructions (Cell Biolabs Inc., CA).

Immunohistochemistry. Paraformaldehyde fixed (4%) and paraffin embedded 4 μm thick liver sections were used. Section were deparaffinized, and antigen retrieval was performed using heat-mediated epitope retrieval solution (ThermoFisher Scientific). Sections were blocked for one hour in PBS containing 3% normal goat serum. Slides were incubated overnight with primary antibodies listed in Supplementary Table 1. Conventional and and multiplex immunostaining showing more than three markers was performed as previously described, and images were analyzed using the trainable classification software Ilastik (v 1.3.3) (Berg et al., Nat Methods. 2019 Dec;16(12):1226-1232. doi: 10.1038/s41592-019-0582-9. Epub 2019 Sep 30) and CellProfiler v3.1.9 (Lamprecht et al., Biotechniques. 2007 Jan;42(1):71-5. doi: 10.2144/000112257) (Guillot et al., Cancers (Basel). 2020 Aug 28;12(9):E2449. doi: 10.3390/cancers12092449).

TUNEL staining. Liver injury was assessed by Terminal deoxynucleotidyl transferase dUTP nick end labeling (TUNEL) staining on formaldehyde fixed paraffin embedded tissue sections as per manufacturer's instructions and revealed either after HRP based coloration (ApopTag Peroxidase In Situ Apoptosis Detection Kit, Millipore Sigma, St. Louis, MO) or by fluorescence (DeadEnd Fluorometric TUNEL System, Promega, Madison, WI).

Liver microcirculation (additional information). Briefly, liver was exposed and scanned by using moorFLPI-2 blood flow imager (Moor Instruments, Wilmington, DE, USA) to determine the red blood cell velocity in 1.5% isoflurane anesthetized mice with core temperatures maintained at 37.2 ± 0.1°C. Hepatic microcirculation was assessed in a 5 mm diametric region of both left and medial lobes placed onto the free part of the liver lobes, and quantified by using the Moor Instruments analysis software. Data are expressed in arbitrary units.

Non-parenchymal cell isolation and FACS analysis. For non-parenchymal collagen-

expressing cell isolation, livers from tamoxifen and ILY injected *ihCD59*$^{BEC\text{-}TG}$ *Coll1*^{GFP} mice were perfused with GBSS containing 0.5 g/L collagenase IV (Millipore Sigma, St. Louis, MO), collected and minced with scissors, and further digested for 20 minutes at 37°C under agitation in GBSS containing 0.5 g/L collagenase IV and 0.5 g/L pronase (Millipore Sigma, St. Louis, MO). Cells were then passed through a 70 µm cell strainer, and HCs were removed after three consecutive low speed centrifugations (60 g 5 minutes). Red blood cells were lysed using ACK Lysing Buffer (ThermoFisher Scientific, Carlsbad, CA). For non-parenchymal immune cell isolation, livers from *ihCD59* or *ihCD59*$^{BEC\text{-}TG}$ mice were excised and cut into small pieces using scissors, before being forced through a 100 µm and a 70 µm cell strainer to obtain single cell suspensions. Hepatocytes were pelleted by low speed centrifugation (60 g 5 minutes) and discarded. Supernatant was centrifuged for 10 minutes at 400 g and pellet was resuspended in 37.5% Percoll solution containing 100 U/mL heparin and centrifuged at 850 g for 30 minutes with the off-brake setting. Red blood cells were lysed using ACK Lysing Buffer (ThermoFisher Scientific, Carlsbad, CA). Pellet was then resuspended, and cells were stained for flow cytometry using fluorochrome-conjugated antibodies listed in Supplementary Table 1 and diluted in PBS+2% FBS.

Quantitative RT-PCR. Total RNA was extracted from snap-frozen liver tissue or cell lysates using the RNeasy Mini Kit (Qiagen, Germantown, MD), following manufacturer's instructions. High-Capacity cDNA Reverse Transcription Kit (ThermoFisher Scientific, Carlsbad, CA) was used for reverse transcription. Real-time PCR was performed on a QuantStudio 6 Flex Real-Time PCR System (ThermoFisher Scientific, Carlsbad, CA), using BrightGreen 2X qPCR MasterMix-ROX (Applied Biological Materials Inc., Richmond, BC). Oligonucleotides used for PCR amplification are listed in Supplementary Table 3.

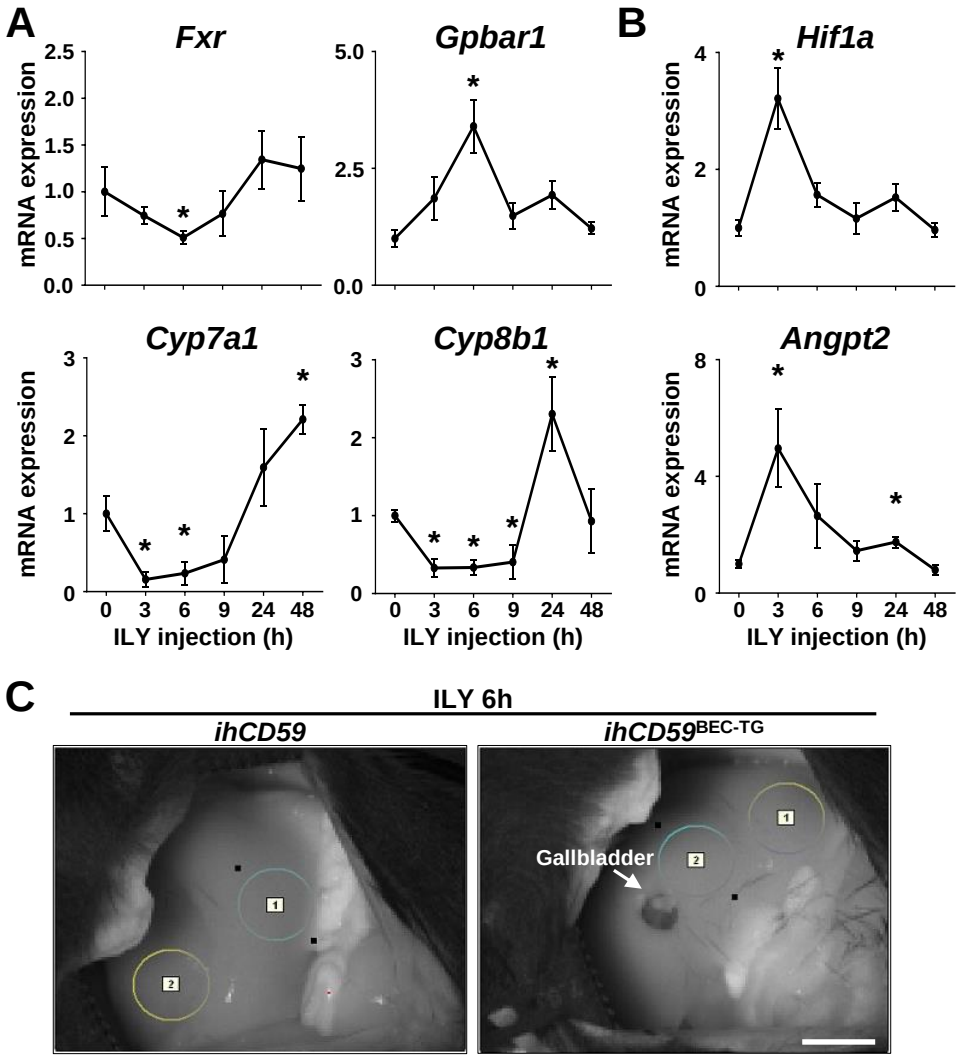

Supplementary Figure 1: Acute BEC death induces cholestasis and liver ischemia
ihCD59 and *ihCD59*$^{BEC\text{-}TG}$ mice were intraperitoneally injected with Tamoxifen (50 mg/kg) to induce hCD59 expression in Sox9^{+} cells, every two days for a total of three injections. Following one-week tamoxifen wash-out period, ILY was injected intravenously (140 µg/kg). Liver samples were collected at the indicated time points post ILY injection for qRT-PCR. **(A)** Alternative representation of quantitative RT-PCR data depicted in Figure 1D (n=3-7). **(B)** Hypoxia-inducible factor 1-alpha (*Hif1a*) and Angiopoietin 2 (*Angpt2*) gene expression were assessed. Data are represented as mean ± SEM. **p*<0.05 as compared to ILY injected *ihCD59* mice (n=3-6 per group). **(C)** Representative grayscale images corresponding to the flux images displayed in Figure 1E, showing the areas of interest (circled and labelled 1 and 2) used for liver blood microcirculation measurements. Scale bar: 5 mm.

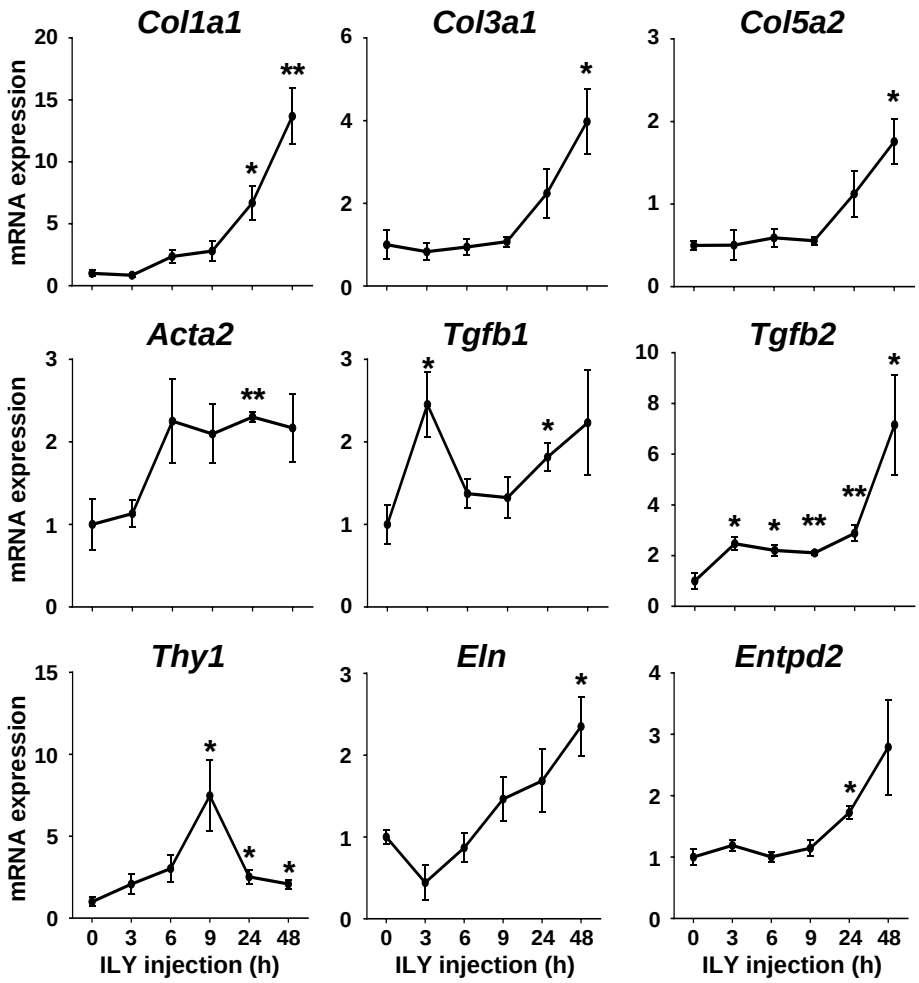

Supplementary Figure 2: Fibrogenesis accompanies bile duct repair after acute injury
ihCD59 and *ihCD59*$^{BEC\text{-}TG}$ mice were treated as described in Supplementary Figure 1. Relative mRNA expression of fibrogenesis-associated genes depicted in Figure 2D. Data are represented as mean ± SEM. *p<0.05; **p<0.01 as compared to *ihCD59* mice (n=3-7 per group).

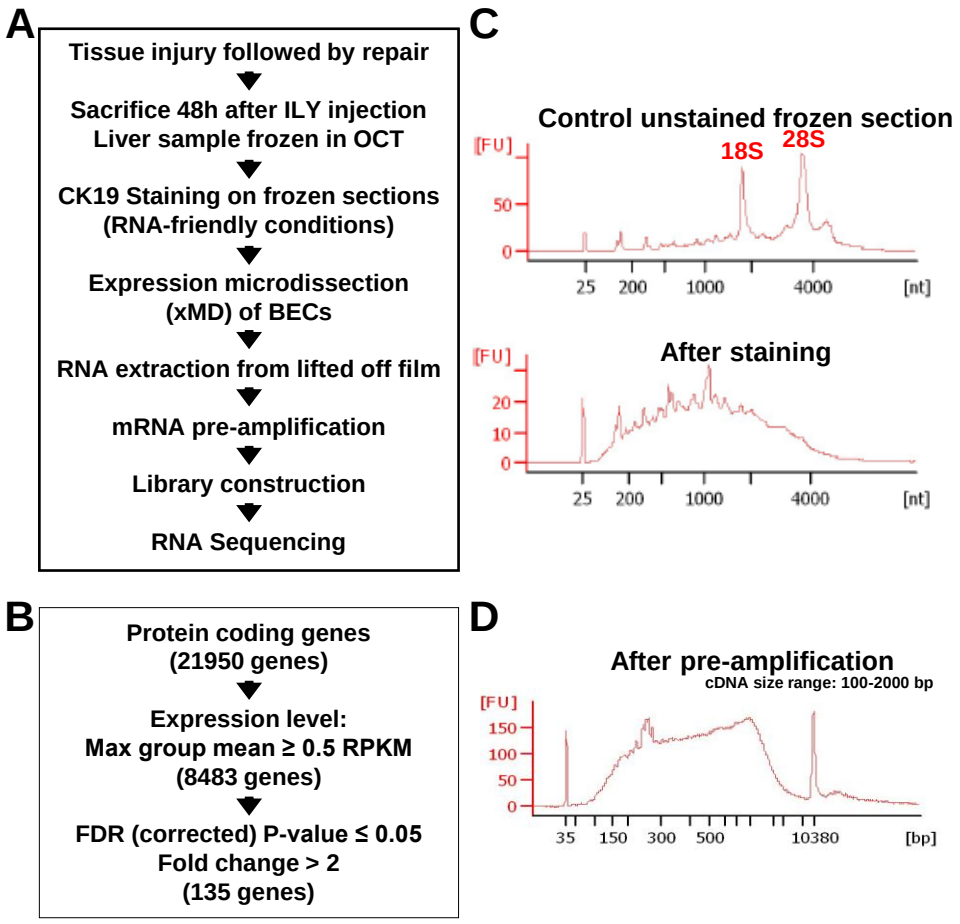

Supplementary Figure 3: Purification and next generation transcriptome (RNAseq) analysis of regenerating BECs

(A) Detailed experimental design. Liver tissue from two *ihCD59* (control group) and two *ihCD59*$^{BEC\text{-}TG}$ (injury group) mice was collected after 48 hours of ILY injection and frozen. Messenger RNA from purified BECs was pre-amplified and sequenced. **(B)** Number of genes throughout RNAseq analysis and filtering pipeline. **(C)** Quality assessment was performed by Bioanalyzer on RNA extracted from unstained or RNA-friendly stained liver tissue sections. Representative plots are shown, revealing acceptable RNA quality after staining (average mRNA length of 1,000 nucleotides shows limited degradation). **(D)** Size profile of pre-amplified mRNA (cDNA) using Ovation RNA-seq System V2. Representative plot.

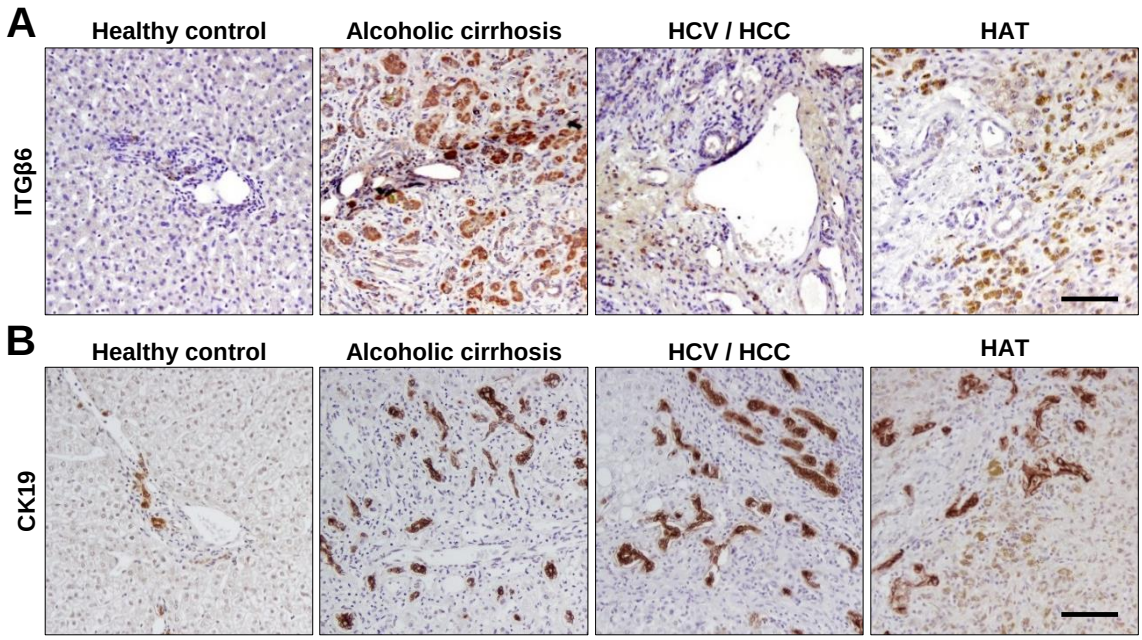

Supplementary Figure 4: Integrin αvβ6 expression is increased in human ductular reaction
Representative images of **(A)** integrin αvβ6 (ITGβ6) and **(B)** cytokeratin-19 (CK19) staining performed on human liver sections of patients suffering from various chronic liver diseases. HCV / HCC: hepatitis C virus infection and hepatocellular carcinoma; HAT: hepatic artery thrombosis. Scale bars: 100 µm.

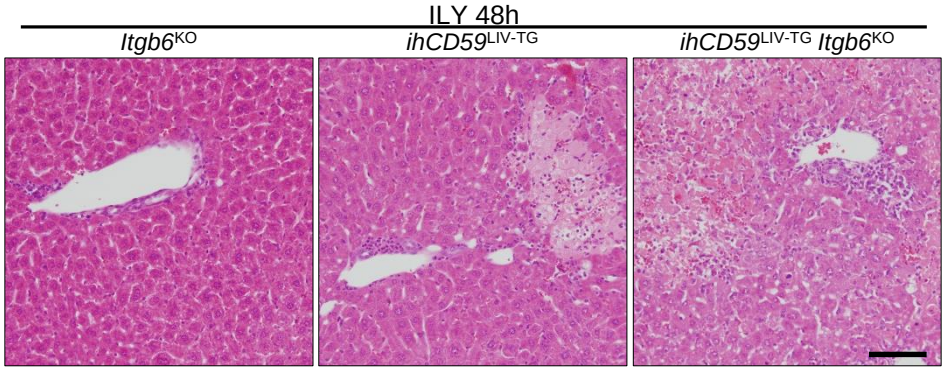

Supplementary Figure 5: Combined acute hepatocyte and BEC death leads to mononuclear cell infiltrates and tissue necrosis.

ihCD59$^{LIV\text{-}TG}$ and *ihCD59*$^{LIV\text{-}TG}$ *Itgb6*^{KO} mice were injected intravenously with ILY, and samples were collected at the indicated time points after ILY injection. Hematoxylin-eosin staining showing tissue injury and inflammation in ILY injected mice. Scale bar: 100 µm.

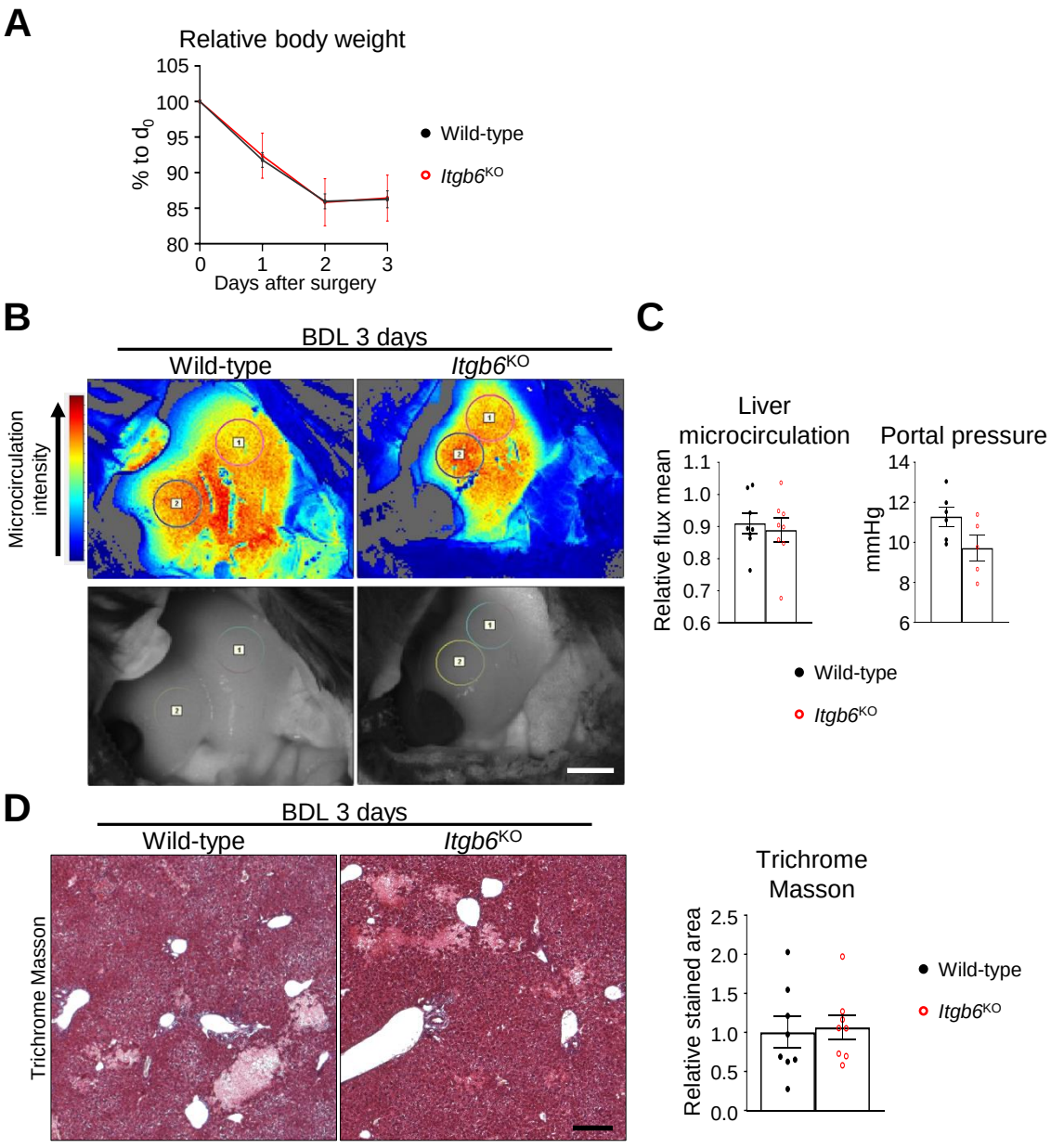

Supplementary Figure 6: Integrin αvβ6 deficiency does not alter early fibrogenesis or liver microcirculation following bile duct ligation

(A) Relative body weight following bile duct ligation surgery performed on wild-type and *Itgb6*^{KO} mice (n=8 per group). **(B)** Liver microcirculation and portal pressure were measured as described in Figure 1E. Representative flux images of wild-type and *Itgb6*^{KO} mice, three days after BDL surgery. Scale bar: 5 mm. **(C)** Relative blood flux mean and portal pressure values. Portal pressure measurement (n=6 wild-type and n=5 *Itgb6*^{KO}). **(D)** Trichrome Masson staining was performed on liver sections, and the stained area was quantified (n=8 per group). Scale bar: 200 µm.

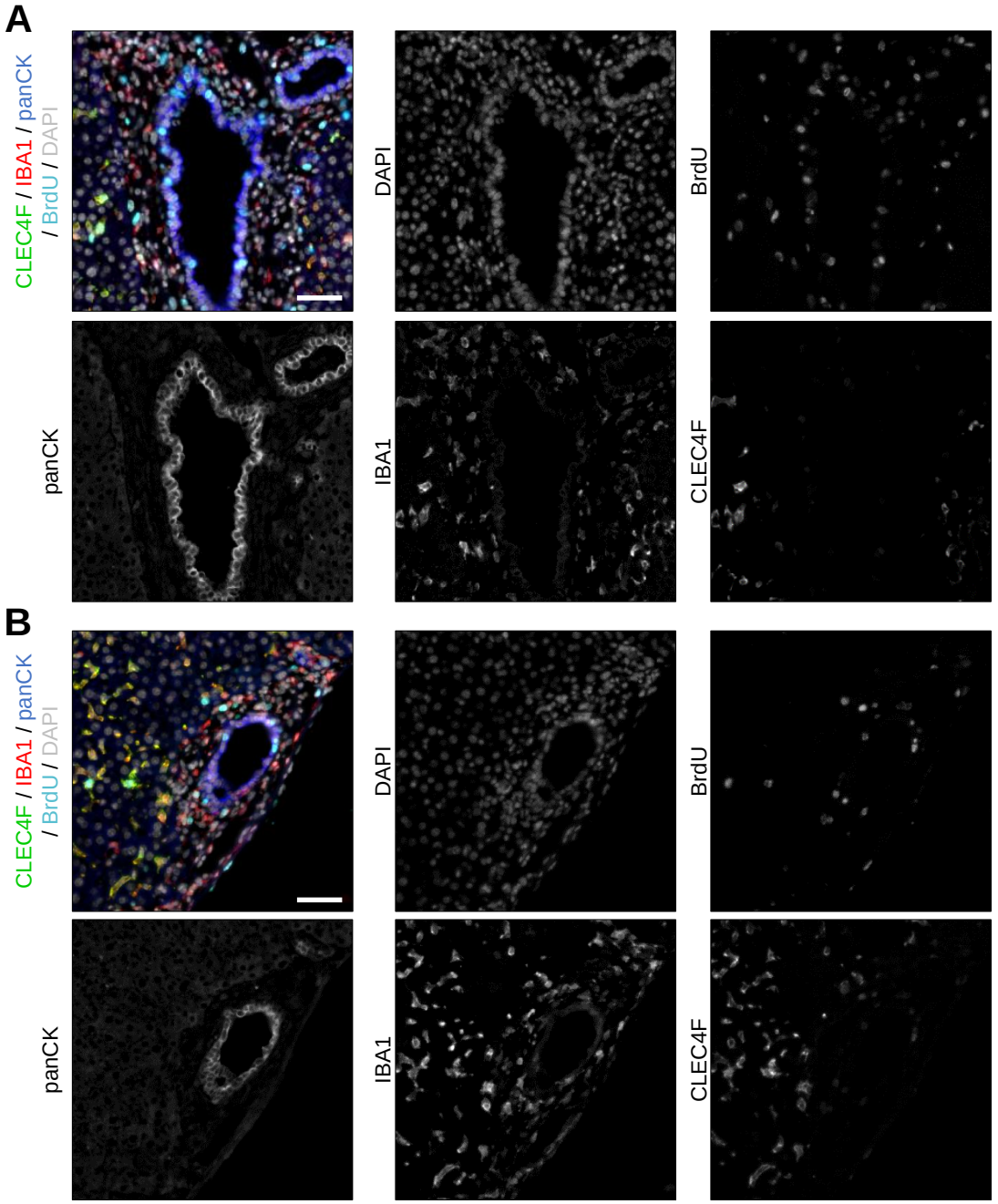

Supplementary Figure 7: Integrin αvβ6 deficiency reduces BEC proliferation following bile duct ligation

Single channel pictures from multiplex fluorescence immunostaining (Figure 5E) are depicted in grayscale, obtained from **(A)** wild-type, or **(B)** *Itgb6*^{KO} FFPE liver, 3 days after bile duct ligation. Scale bars: 50 µm.

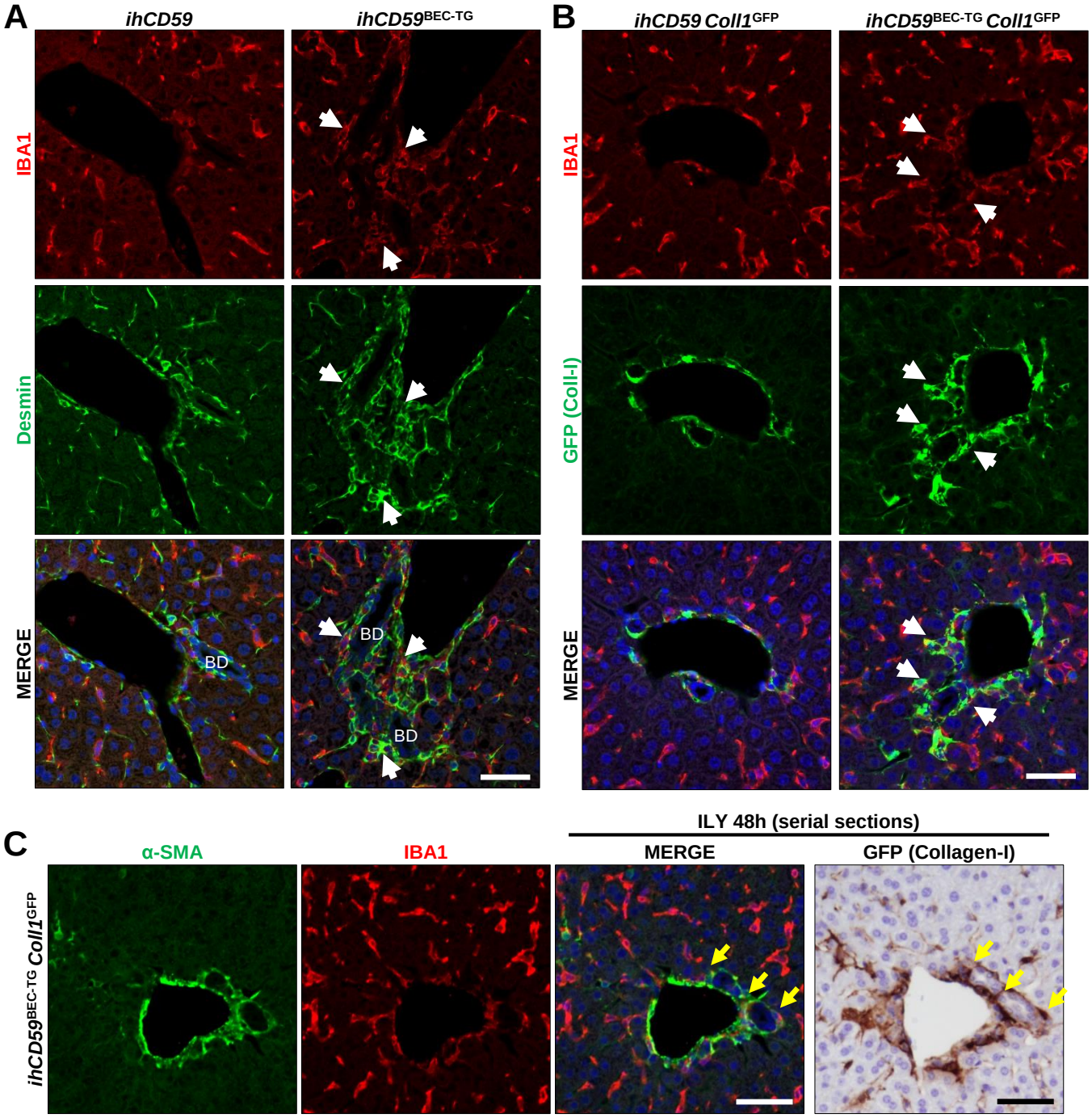

Supplementary Figure 8: Monocytes and fibrogenic cells are in close interaction during bile duct repair.

Single channel pictures from data presented in Figure 6A-C. **(A)** IBA1 (red) and Desmin (green), and **(B)** IBA1 (red) GFP (Collagen-I, green) immunostaining was performed, 48 hours after ILY administration. **(C)** IBA1 (red) and α-SMA (green) co-staining, and GFP (collagen-I) staining were performed on serial liver sections from *ihCD59*$^{BEC\text{-}TG}$ *Coll1*^{GFP} mice, 48h after ILY injection. Yellow arrows indicate cell clusters of IBA1^{+}, α-SMA^{+} and GFP^{+} cells. Scale bars: 50 µm.

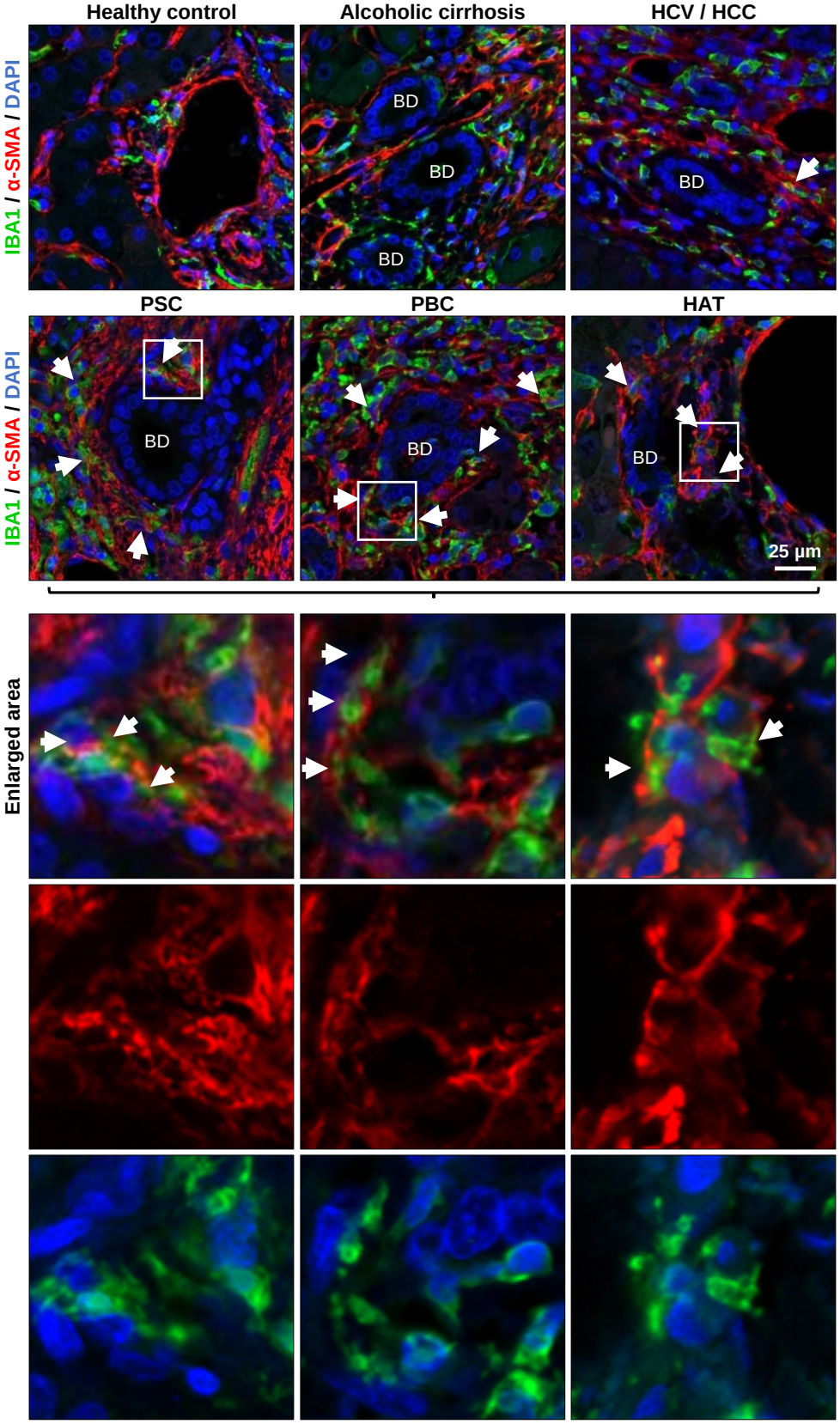

Supplementary Figure 9: IBA1⁺ macrophages and α-SMA⁺ fibroblasts accumulate around injured bile ducts in patients suffering liver disease of various etiologies

Representative images of IBA1 (green) and α-SMA (red) staining performed on various chronic liver diseases from patients. An enlarged area with single channel pictures is depicted in the lower panel. White arrows indicate positive cell clusters. Quantification is depicted in Figure 6D. BD: bile duct-like structures; HCV/HCC: Hepatitis C virus infection and hepatocellular carcinoma; PSC: primary sclerosing cholangitis; PBC: primary biliary cholangitis; HAT: hepatic artery thrombosis.

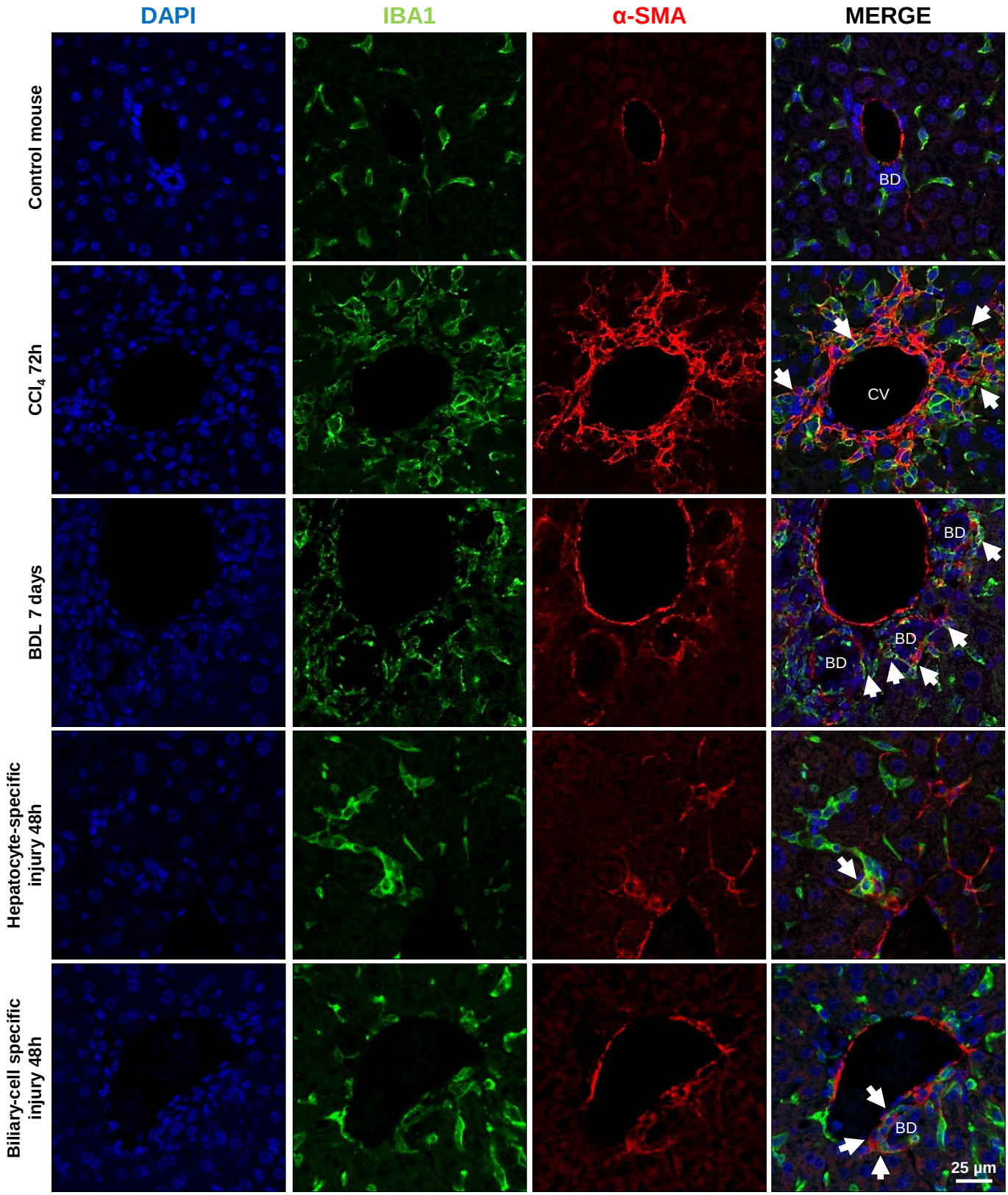

Supplementary Figure 10: IBA1⁺ macrophages and α-SMA⁺ fibroblasts accumulate around injured bile ducts in different murine models of liver injury

Representative images of the IBA1 (green) and α-SMA (red) staining performed on mouse samples from different liver injury models. Quantification is depicted in Figure 6D. White arrows indicate double positive cells. CV: central vein, BD: bile duct-like structures, BDL: Bile duct ligation and section.

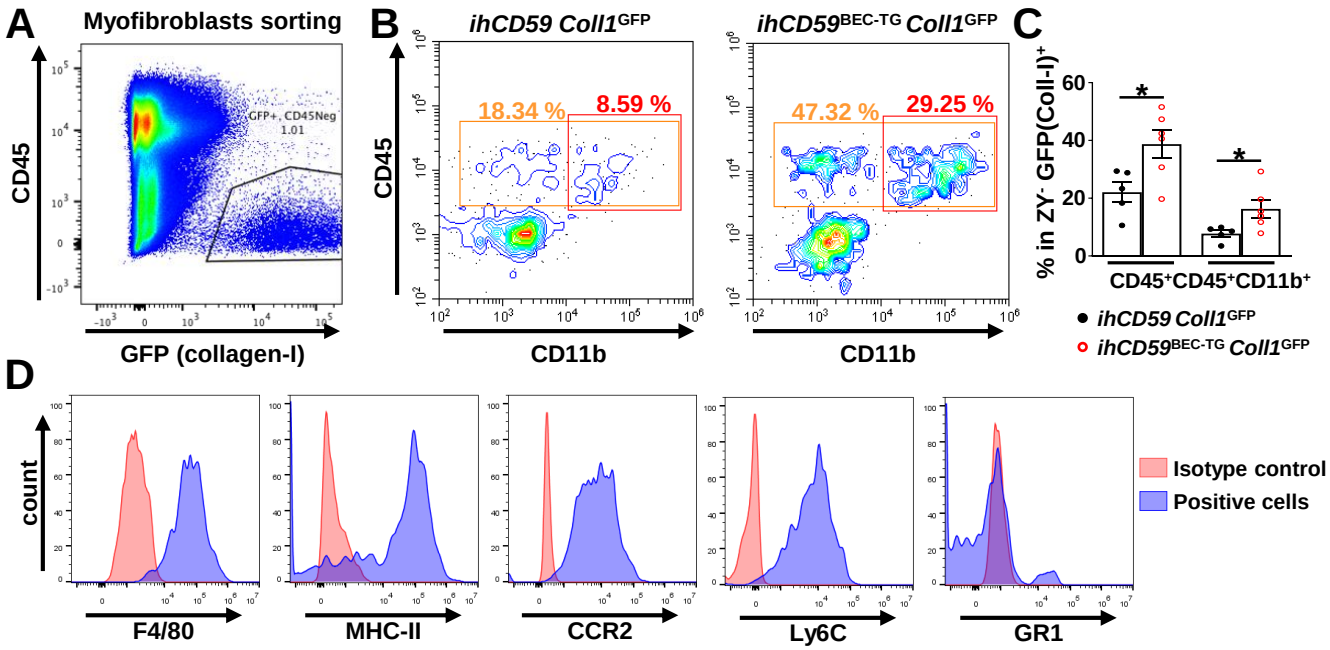

Supplementary Figure 11: Monocytes, an alternative source of fibrogenic cells?
(A) Collagen-I producing (GFP^{+}) CD45^{NEG} fibroblasts were sorted from carbon tetrachloride (CCl_4) injected *Coll1*^{GFP} mouse livers. **(B)** *ihCD59*$^{BEC\text{-}TG}$*Coll1*^{GFP} mice were injected with ILY, and euthanized 48 hours after ILY injection. Representative flow cytometry data obtained from liver non-parenchymal cell fraction analysis are shown. After doublets exclusion and SSC/FSC gating, live (Zombie Yellow negative) and GFP (collagen-I) -positive cells were assessed for CD45 and CD11b expression. **(C)** Flow cytometry results from 5-6 mice per group show percentages of ZY^{-}GFP^{+}CD45^{+} and ZY^{-}GFP^{+}CD45^{+}CD11b^{+} among ZY^{-}GFP^{+} cells. **(D)** Representative F4/80, MHC-II, CCR2, Ly6C and GR1 expression in ZY^{-}GFP^{+}CD45^{+}CD11b^{+} cells from *ihCD59*$^{BEC\text{-}TG}$*Coll1*^{GFP} mice as assessed by FACS, 48 hours after ILY injection. *p<0.05 as compared to control *ihCD59Colll*^{GFP} mice, unpaired Student's t test (n=5-6 per group).

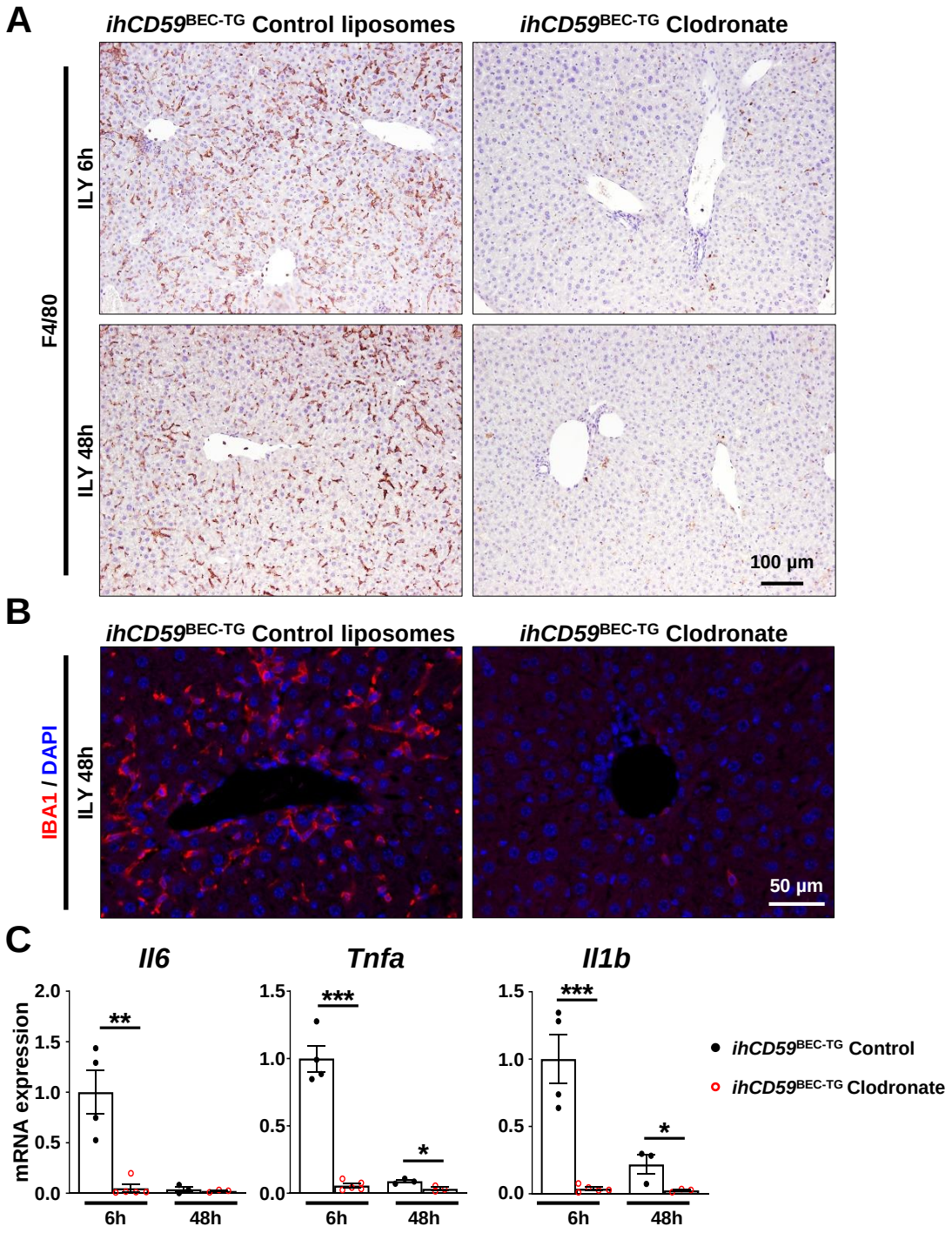

Supplementary Figure 12: Liver inflammation is impaired after macrophage depletion using clodronate-loaded liposomes

Following tamoxifen injections and wash out period, macrophages were depleted using clodronate-loaded liposomes 24 hours prior to ILY injection. Macrophage depletion was verified by **(A)** F4/80 immunostaining, and **(B)** IBA1 immunostaining. **(C)** Inflammation-related relative gene expression was assessed on liver homogenates by qRT-PCR. Data are represented as mean ± SEM. *p<0.05; **p<0.01; ***p<0.005 as compared to control liposome injected mice, unpaired Student's t test (n=3-5 per group).

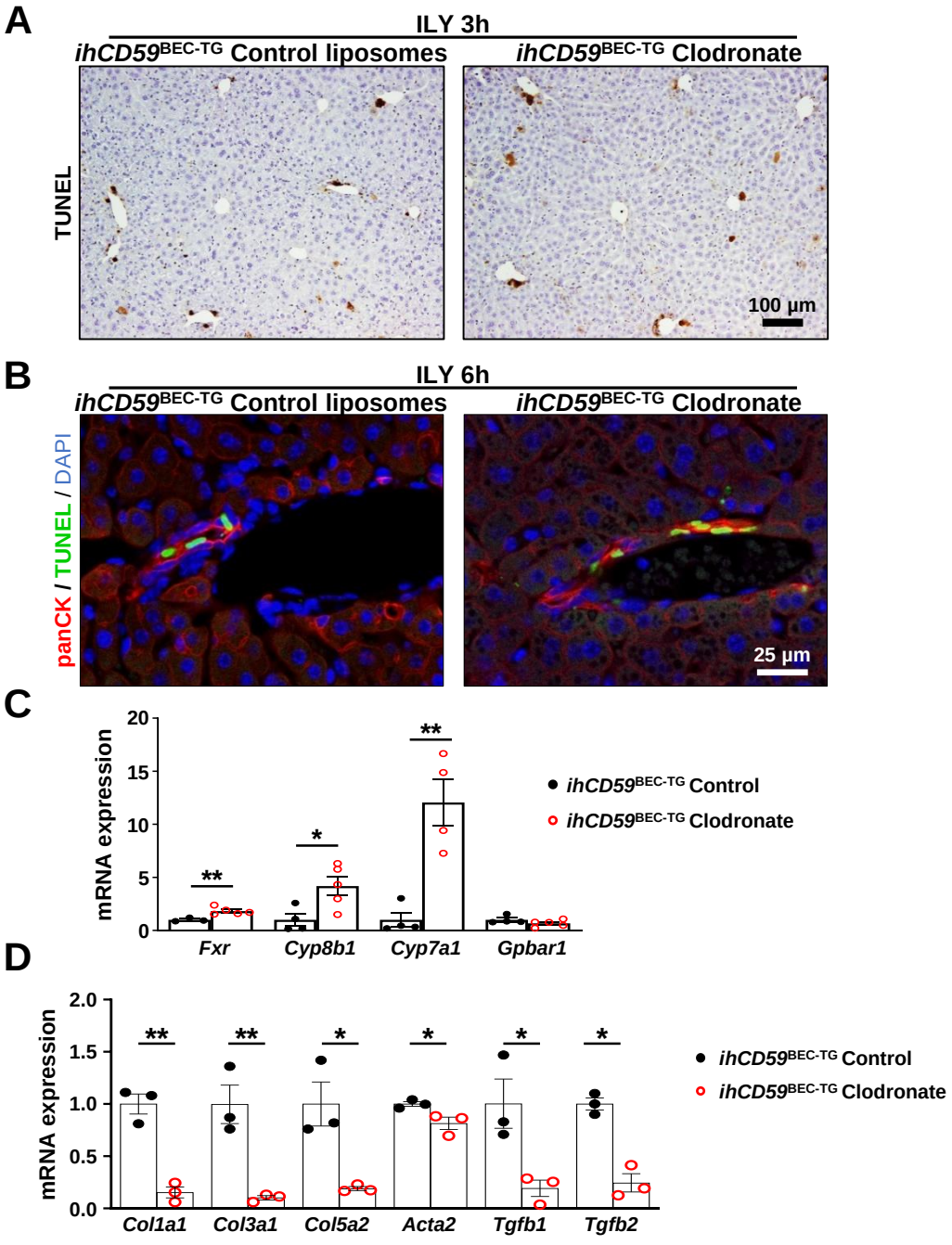

Supplementary Figure 13: Macrophage depletion reduces cholestasis and bile duct repair after BEC injury (representative fields)

(A) TUNEL, and **(B)** panCK (red) TUNEL (green) representative images used for the quantifications presented in Figure 7A. **(C)** Quantitative RT-PCR data depicted in Figure 7C. **(D)** Quantitative RT-PCR data depicted in Figure 7E. Data are represented as mean ± SEM. *p<0.05; **p<0.01 as compared to control liposome injected *ihCD59*$^{BEC-TG}$ mice, unpaired Student's t test (n=3-5 per group).

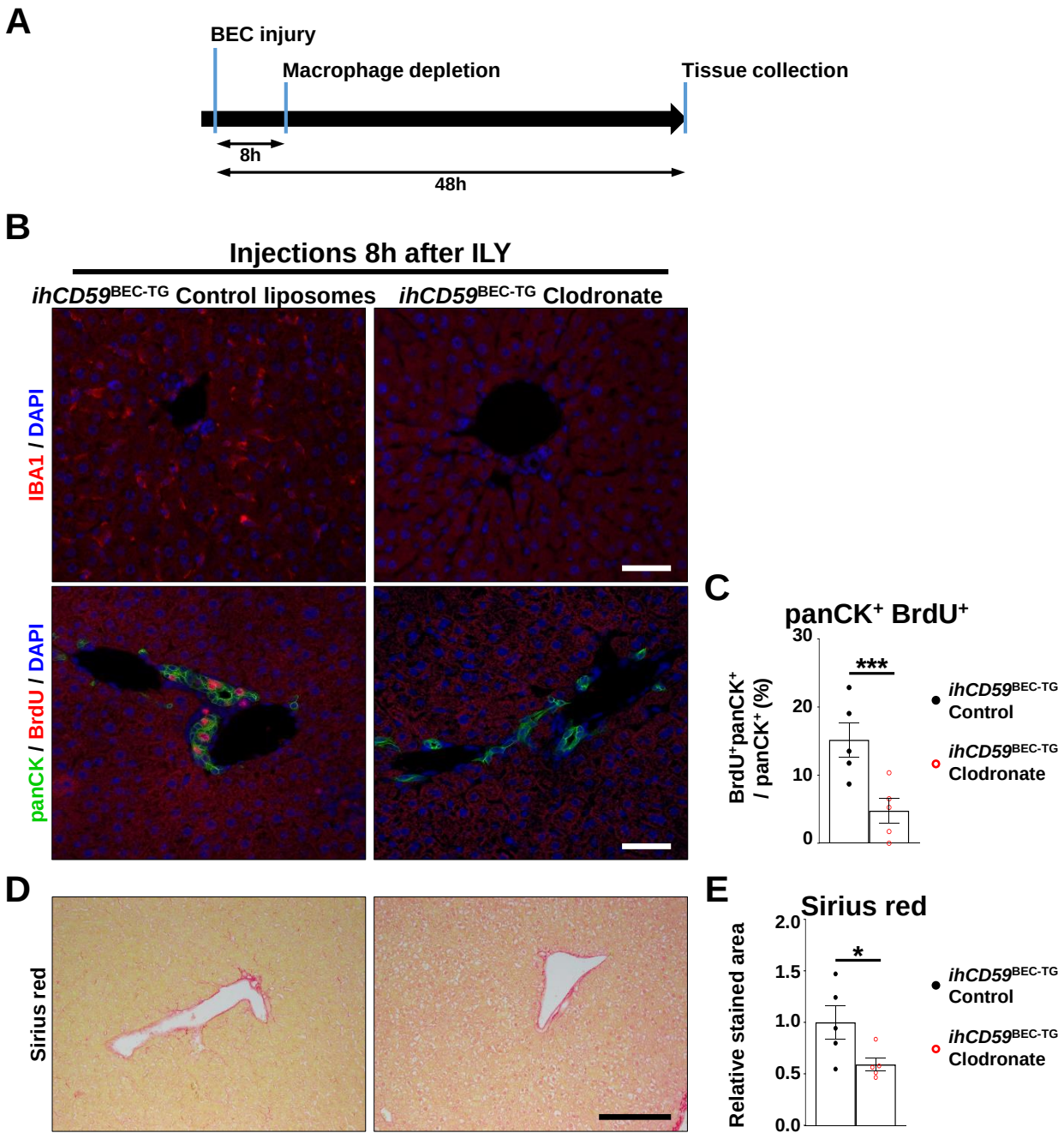

Supplementary Figure 14: Macrophage depletion 8 hours after ILY injection reduces BEC proliferation

(A) Experimental design: Mice were injected with clodronate-loaded or control liposomes 8 hours after ILY injection. Tissues were collected 48 hours after the initial BEC injury. **(B)** IBA1 (red, upper panel), panCK and BrdU (green and red, respectively, lower panel) were performed on liver sections obtained from control- or clodronate-loaded liposome injected mice. Scale bars: 50 µm. **(C)** Quantification of proliferating BECs. **(D)** Sirius red staining was performed (scale bar: 200 µm), and **(E)** relative stained area was quantified in both groups. **p<0.01; ***p<0.005 as compared to control liposome injected *ihCD59*$^{BEC\text{-}TG}$ mice, unpaired Student's t test (n=5 per group).

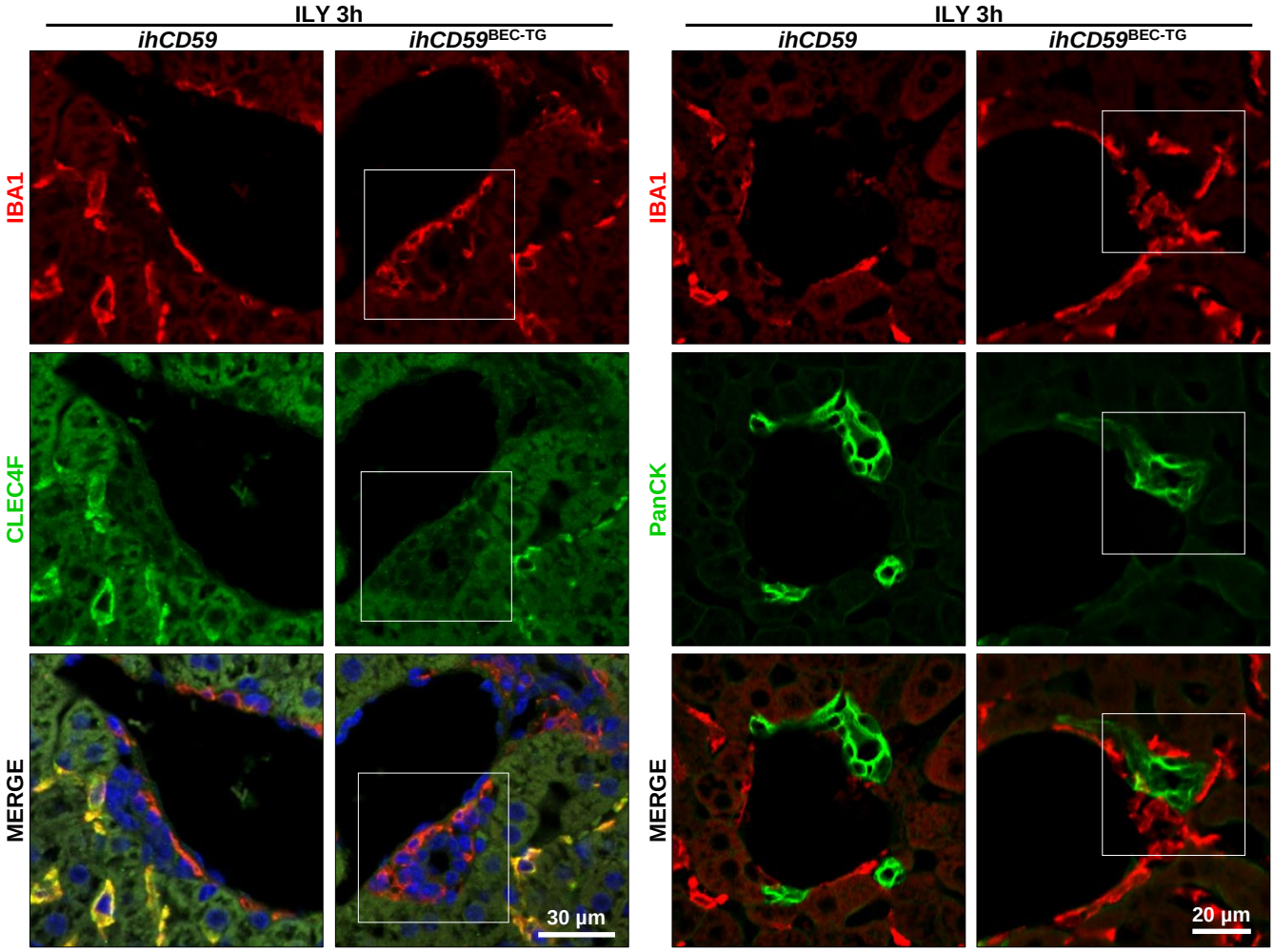

Supplementary Figure 15: Monocytes are recruited around damaged bile ducts following acute BEC injury

IBA1 (red) and CLEC4F (green, left panel) or pan-cytokeratin (PanCK, right panel in green) immunostaining was performed on liver sections, 3 hours after ILY injection. Single channel images of the representative fields presented in Figure 8A.

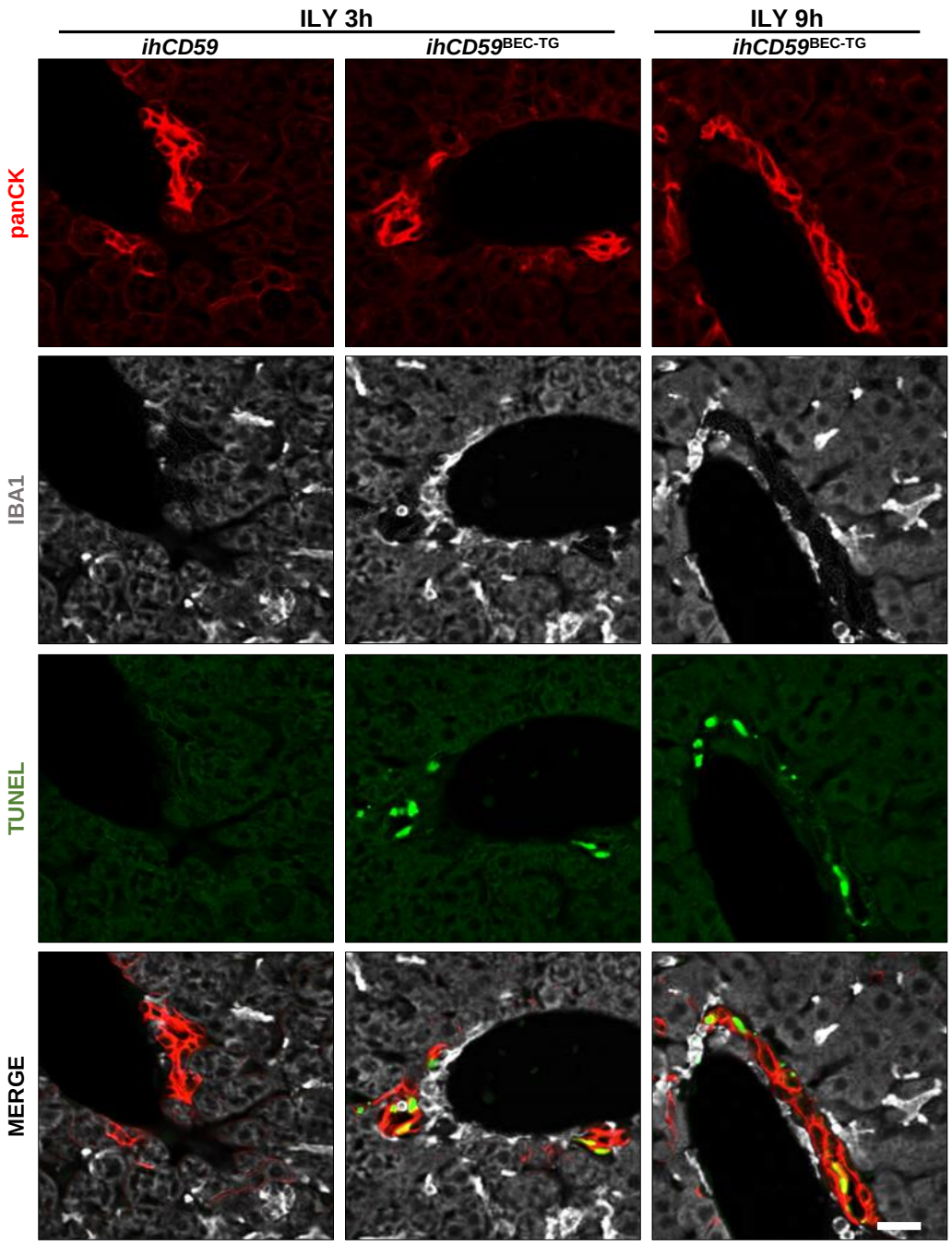

Supplementary Figure 16: Recruited monocytes accumulate around injured BECs
ihCD59$^{BEC\text{-}TG}$ mice were treated as described in Supplementary Figure 1. Liver tissue sections (Formalin-Fixed Paraffin-Embedded) were subjected to immunostaining. Representative immunostaining showing monocyte (IBA1, grey) accumulation in contact with damaged BECs (panCK, red and TUNEL, green). Scale bar: 20 µm.

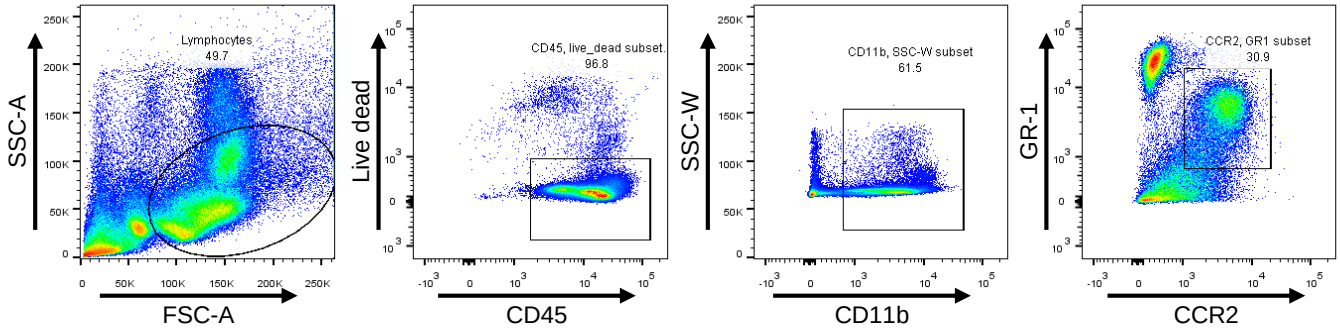

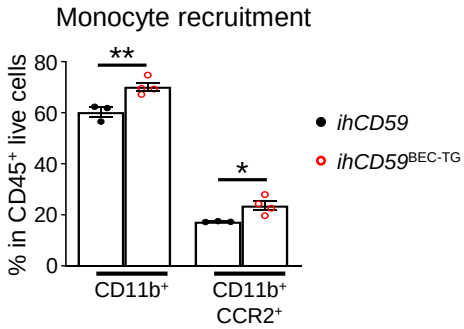

Supplementary Figure 17: Circulating monocytes are recruited in the liver after acute biliary epithelial cell injury

Non-parenchymal cells were isolated and hepatocytes, $CD3^+$ and $CD19^+$ cells were removed. $CCR2^+$ $CD11b^+$ cells in the $CD45^+$ cell population was evaluated by flow cytometry. *p<0.05; **p<0.01 as indicated, unpaired Student's t test (n=3-4 per group).

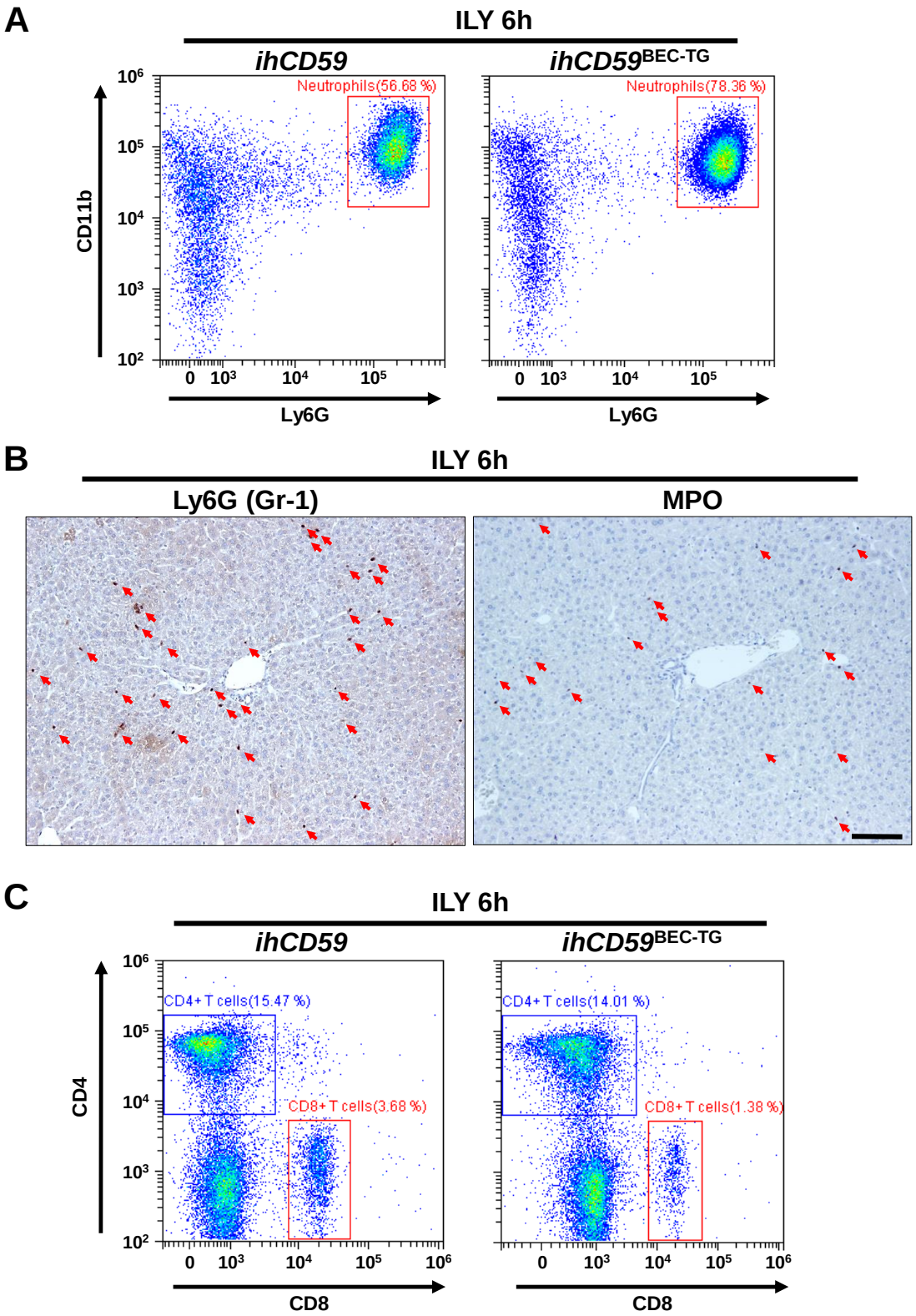

Supplementary Figure 18: Neutrophils accumulate in the liver after BEC injury, but not in the vicinity of bile ducts while T lymphocytes do not seem to be involved

(A) Non-parenchymal liver cells were isolated and analyzed by FACS staining, 6 hours after ILY injection. Neutrophils were identified as Zombie Yellow^{-} CD45^{+} CD3^{-} CD19^{-} CD11b^{+} Ly6G^{+} cells. **(B)** Paraffin embedded liver sections from *ihCD59*$^{BEC\text{-}TG}$ mice were stained for Ly6G (left panel) or myeloperoxidase (MPO, right panel) to reveal neutrophil localization. Scale bar: 100 µm. **(C)** Leukocytes were gated as Zombie Yellow^{-} CD45^{+} CD3^{+}, and CD4^{+} or CD8a^{+} T-lymphocyte recruitment was evaluated.

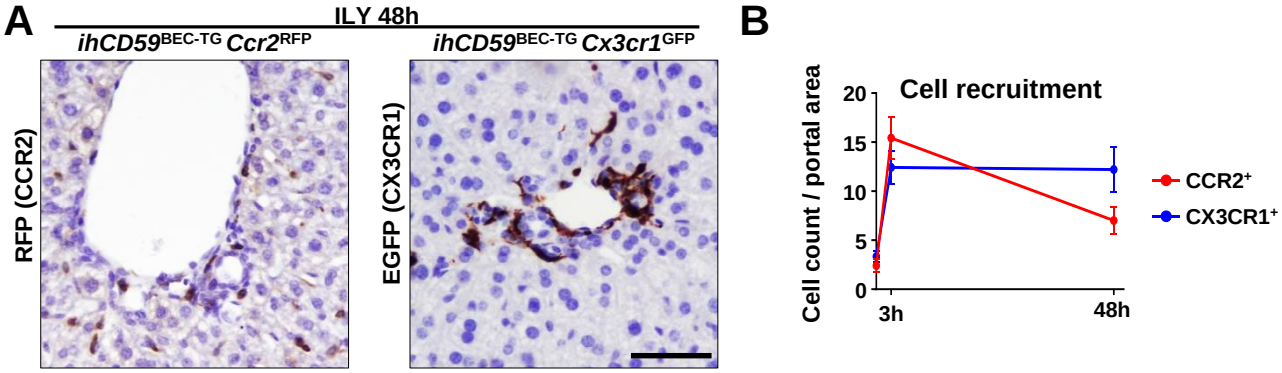

Supplementary Figure 19: Freshly recruited monocytes accumulate around injured BECs 48 hours post-injury

ihCD59 Cx3cr1^{GFP}*, ihCD59*$^{BEC\text{-}TG}$ *Cx3cr1*^{GFP}*, ihCD59 Ccr2*^{RFP} *and ihCD59*$^{BEC\text{-}TG}$*Ccr2*^{RFP} mice were treated as described in Supplementary Figure 1. Liver tissues were subjected to immunostaining. **(A)** GFP or RFP immunostaining, as appropriate. **(D)** GFP^{+} or RFP^{+} cell count, showing CCR2^{+} or CX3CR1^{+} cell accumulation in portal areas (n=5-7 per group). Scale bar: 50 µm.

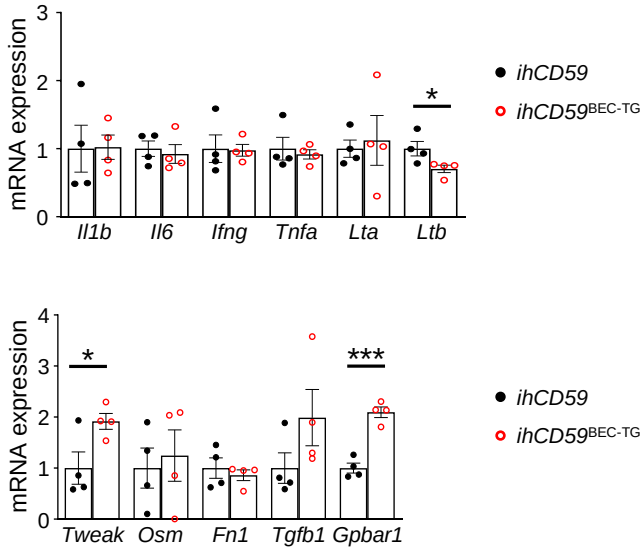

Supplementary Figure 20: Macrophage characterization during bile duct repair
Liver macrophages were isolated from *ihCD59* and *ihCD59*$^{BEC\text{-}TG}$ mice, 48 hours after ILY injection. Gene expression analysis was performed by qRT-PCR. Statistical analysis of qRT-PCR data shown in Figure 6J. *p<0.05; ***p<0.005 as indicated, unpaired Student's t test (n=4 per group).

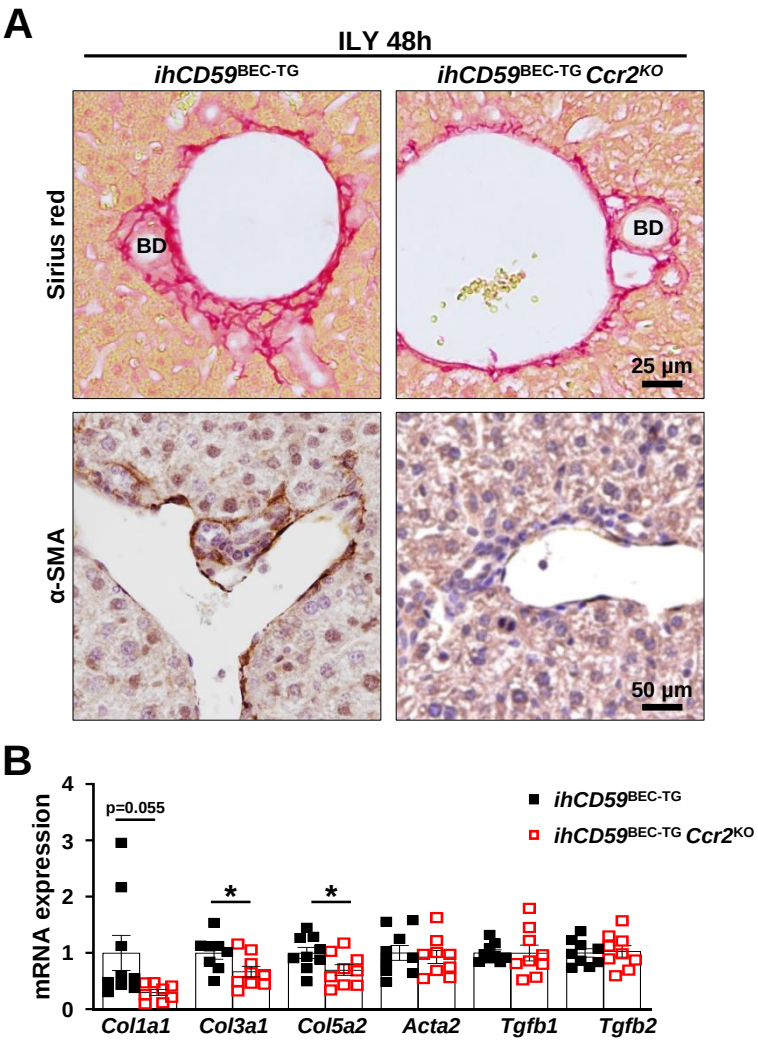

Supplementary Figure 21: Macrophage depletion or Ccr2-deficiency reduces portal fibrosis in a model of acute and targeted biliary epithelial cell death

ihCD59$^{BEC\text{-}TG}$ and *ihCD59*$^{BEC\text{-}TG}$ *Ccr2*^{KO} mice were also injected with ILY and liver tissue was collected after 48 hours. **(A)** Representative pictures obtained after Sirius red, α-SMA or PanCK (green) and BrdU (red) staining used for quantification in Figure 8F. **(B)** Statistical analysis of qRT-PCR data shown in Figure 8G, **p*<0.05; ***p*<0.01 as indicated, unpaired Student's t test (n=8-9 per group).

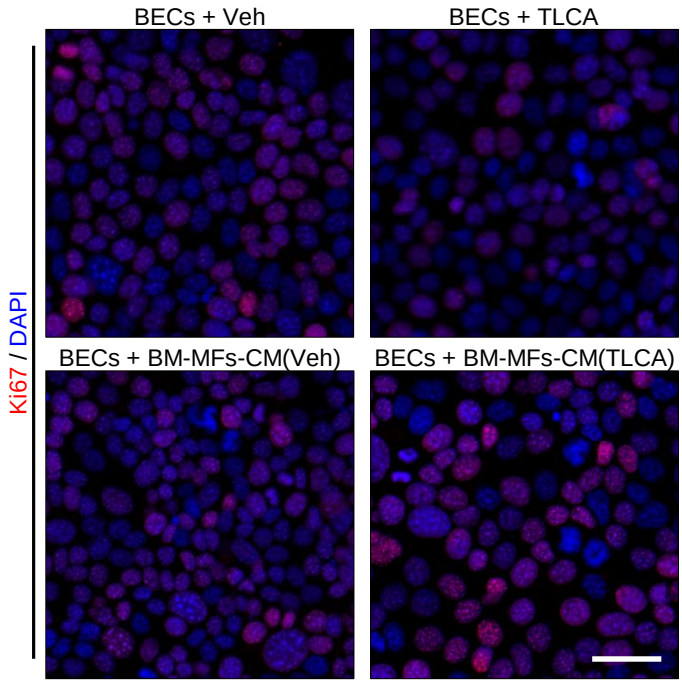

Supplementary Figure 22: Cultured BECs proliferation is increased in the presence of bile acid-activated macrophages.
Conditionned-media from TLCA-treated bone-marrow derived macrophages (BM-MFs-CM) was added to BECs for 24 hours, and Ki67 staining was performed. Scale bar: 40 µm.

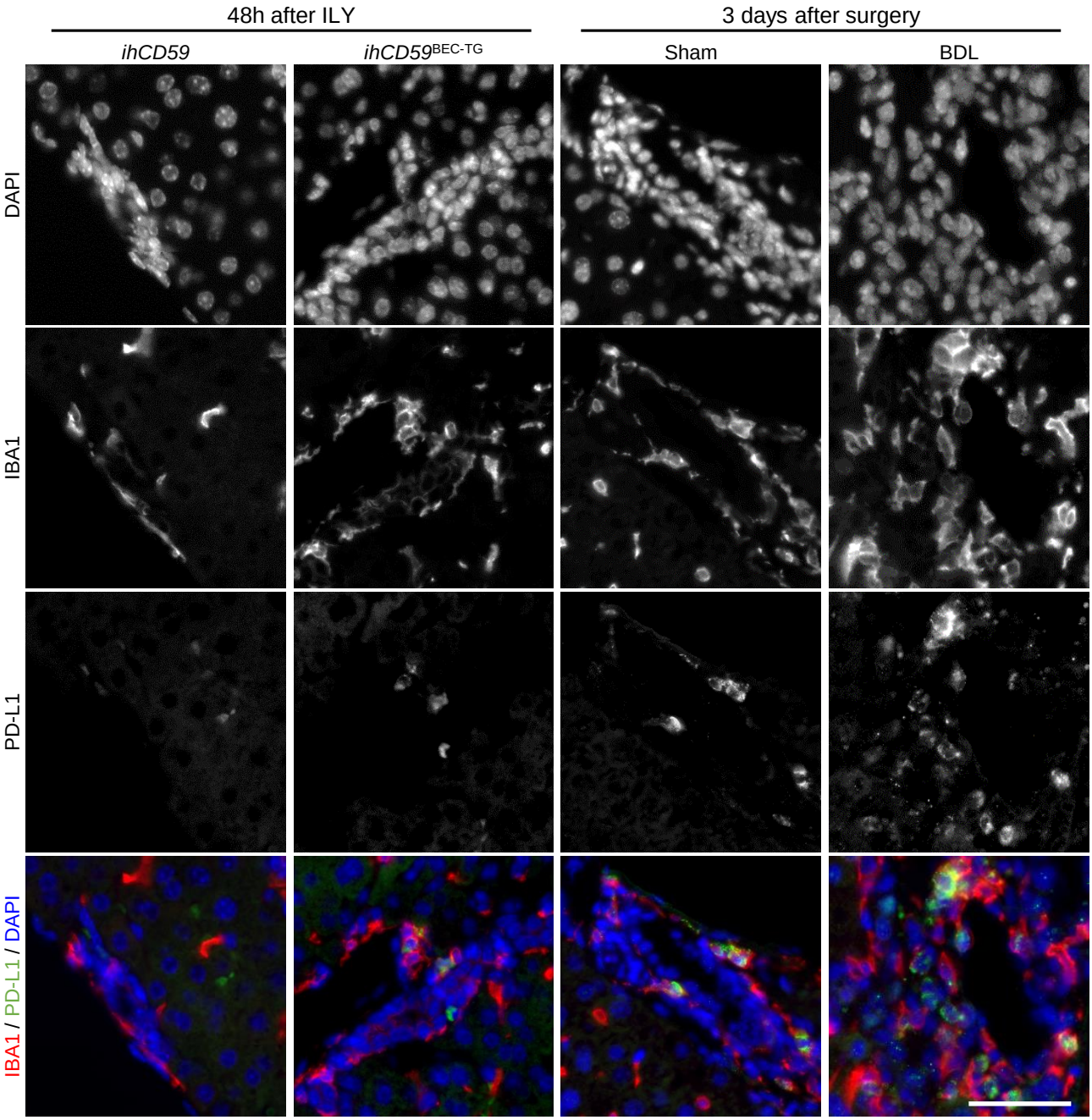

Supplementary Figure 23: PD-L1⁺ macrophages accumulate around bile ducts
Liver FFPE section from mice that were injected with ILY and killed 48 hours later, or 3 days after sham or BDL-surgery, were subjected to IBA1 (red) and PD-L1 (green) immunostaining. Corresponding single channel pictures from Figure 4D are shown. Scale bar: 50 µm.

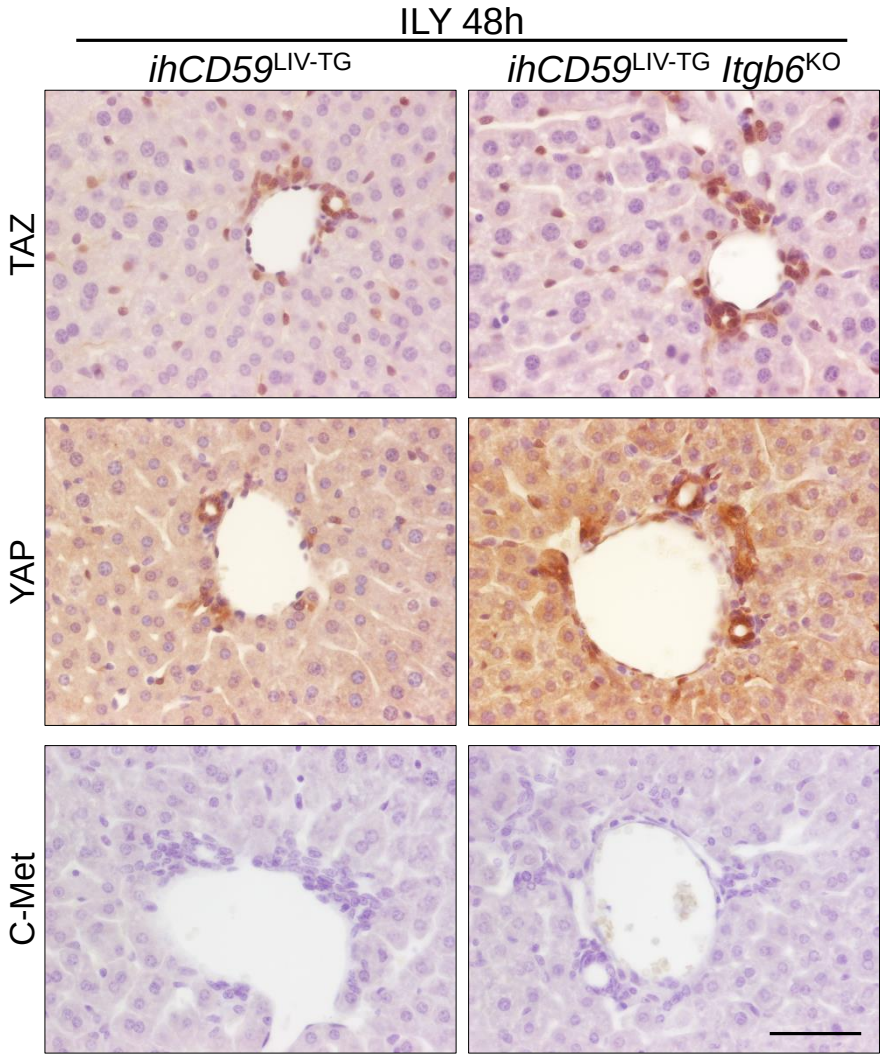

Supplementary Figure 24: YAP/TAZ and cMet signaling are not altered in *ihCD59*$^{LIV-TG}$ *Itgb6*^{KO} animals

Liver FFPE section from *ihCD59*$^{LIV-TG}$, or *ihCD59*$^{LIV-TG}$ *Itgb6*^{KO} mice sacrificed 48 hours after ILY injection, were stained for TAZ, YAP, and cMet. Scale bar: 100 µm.

Antigen	Application(s)	Manufacturer	Catalog #	Host species	Dilution
BrdU	IHC-P	BD Biosciences, San Jose, CA	550803	Biotin-conjugated	1/20
BrdU	IHC-P	Abcam, Cambridge, UK	6326	Rat	1/200
c-MET	IHC-P	R&D Systems, Minneapolis, MN	AF2480	Rabbit	1/200
CCR2	FC	BioLegend, San Diego, CA	150604	Rat	1/200
CD11b	FC	BD Biosciences, San Jose, CA	550993	Rat	1/200
CD11b	FC	ThermoFisher Scientific, Carlsbad, CA	45-0112-82	Rat	1/200
CD3	FC	BioLegend, San Diego, CA	100216	Rat	1/200
CD4	FC	ThermoFisher Scientific, Carlsbad, CA	47-0042-80	Rat	1/200
CD8a	FC	BD Biosciences, San Jose, CA	553031	Rat	1/200
CD45	FC	ThermoFisher Scientific, Carlsbad, CA	25-0451-82	Rat	1/200
CD45	FC	ThermoFisher Scientific, Carlsbad, CA	69-0451-82	Rat	1/200
CK19	IHC-P, xMD	Developmental Studies Hybridoma Bank, Iowa City, IA *	TROMA-III	Rat	1/4
CLEC4F	IHC-P	R&D Systems, Minneapolis, MN	MAB2784	Rat	1/200
Desmin	IHC-P	Abcam, Cambridge, UK	ab15200	Rabbit	1/100
F4/80	FC	ThermoFisher Scientific, Carlsbad, CA	12-4801-82	Rat	1/200
F4/80	IHC-P	Bio-Rad , Hercules, CA	MCA497R	Rat	1/500
GFP	IHC-P	Cell Signaling , Danvers, MA	2955	Mouse	1/100
GFP	IHC-P	Cell Signaling , Danvers, MA	2956	Rabbit	1/400
IBA1	IHC-P	VWR, Arlington Heights, IL	100369-764	Rabbit	1/1,000
IBA1	IHC-P	Millipore Sigma, St. Louis, MO	MABN92-25UG	Mouse	1/500
ITGB6	IHC-P	ProteinTech, Chicago, IL	19695	Rabbit	1/100
Ki67	ICC	Dako by Agilent, Santa Clara, CA	M7249	Rat	1/100
Ly6C	FC	BioLegend, San Diego, CA	128024	Rat	1/200
Ly6G / Gr1	IHC-P	BioXCell, West Lebanon, NH	BE0075	Rat	1/100
Ly6G / Gr1	FC	ThermoFisher Scientific, Carlsbad, CA	17-9668-80	Rat	1/200
Ly6G / Gr1	FC	ThermoFisher Scientific, Carlsbad, CA	48-9668-82	Rat	1/200
MHC-II	FC	ThermoFisher Scientific, Carlsbad, CA	47-5321-82	Rat	1/200
MPO	IHC-P	Biocare Medical , Concord, CA	PP023AA	Rabbit	RTU
panCK	IHC-P	Cell Signaling , Danvers, MA	4545	Mouse	1/500
panCK	IHC-P	Agilent Dako, Santa Clara, CA	Z0622	Rabbit	1/200
PD-L1	IHC-P	Cell Signaling , Danvers, MA	64988S	Rabbit	1/200
RFP	IHC-P	Rockland, PA	600-401-379	Rabbit	1/250
TAZ	IHC-P	Cell Signaling , Danvers, MA	72804	Rabbit	1/200
YAP	IHC-P	Cell Signaling , Danvers, MA	14074	Rabbit	1/400
α-SMA	IHC-P	Agilent Dako, Santa Clara, CA	M085129-2	Mouse	1/200

Supplementary Table 1: Primary antibodies used in this study

FC: Flow cytometry; IHC-P: immunohistochemistry paraffin sections; xMD: expression microdissection. The monoclonal anti-mouse cytokeratin-19 (CK19/TROMA-III) antibody developed by R. Kemler, was obtained from the Developmental Studies Hybridoma Bank developed under the auspices of the NICHD and maintained by The University of Iowa, Department of Biology (Iowa City, IA 52242).

	Category	Term	Count	%	Fold Enrichment	PValue	Benjamini	Genes
Induced	GOTERM_CC_DIRECT	GO:0005576~extracellular region	16	28.6	5.2	1.39E-07	1.84E-05	CCL2, LAD1, COL3A1, CLU, APOC2, NID1, TRF, APOA4, LCN2, ANGPTL8, MUP20, SAA2, HPX, SAA1, COL1A1, ORM2
	GOTERM_CC_DIRECT	GO:0005615~extracellular space	15	26.8	4.6	1.60E-06	1.06E-04	CCL2, COL3A1, CLU, APOC2, SELENBP2, TRF, APOA4, LCN2, MUP20, SAA2, HPX, LRG1, SAA1, COL1A1, ORM2
	GOTERM_CC_DIRECT	GO:0005578~proteinaceous extracellular matrix	5	8.9	11.7	7.80E-04	0.034	LAD1, COL3A1, TGM2, NID1, COL1A1
	GOTERM_BP_DIRECT	GO:0031100~organ regeneration	4	7.1	16.5	1.65E-03	0.582	CDKN1A, CCL2, MKI67, FLT3
	GOTERM_BP_DIRECT	GO:0034364~high-density lipoprotein particle	3	5.4	22.0	7.70E-03	0.225	APOA4, SAA2, SAA1
	GOTERM_BP_DIRECT	GO:0070328~triglyceride homeostasis	3	5.4	20.3	9.02E-03	0.909	APOA4, ANGPTL8, APOC2
	GOTERM_CC_DIRECT	GO:0031012~extracellular matrix	5	8.9	5.4	0.013	0.285	COL3A1, CLU, TGM2, NID1, COL1A1
	GOTERM_BP_DIRECT	GO:0006953~acute-phase response	3	5.4	16.5	0.013	0.908	SAA2, SAA1, ORM2
	GOTERM_BP_DIRECT	GO:0009611~response to wounding	3	5.4	16.5	0.013	0.908	CCL2, ABHD2, ID3
	GOTERM_BP_DIRECT	GO:0072562~blood microparticle	4	7.1	7.8	0.014	0.261	APOA4, HPX, CLU, TRF
	GOTERM_BP_DIRECT	GO:0060326~cell chemotaxis	3	5.4	15.4	0.015	0.872	CCL2, SAA2, SAA1
	KEGG_PATHWAY	mmu04512:ECM-receptor interaction	3	5.4	14.4	0.016	0.705	COL3A1, ITGB6, COL1A1
	GOTERM_CC_DIRECT	GO:0005913~cell-cell adherens junction	6	10.7	3.9	0.017	0.277	KRT18, LAD1, DIAPH3, ANLN, TAGLN2, EPS8L2
	GOTERM_CC_DIRECT	GO:0070062~extracellular exosome	18	32.1	1.7	0.017	0.249	LAD1, CLU, APOC2, NID1, SELENBP2, TAGLN2, TRF, APOA4, LCN2, KRT18, SAA2, HPX, LRG1, SAA1, ITGB6, KRT8, TGM2, EPS8L2
	GOTERM_BP_DIRECT	GO:0007067~mitotic nuclear division	5	8.9	4.9	0.017	0.844	KIF23, NEK3, ANLN, CENPE, HAUS8
	GOTERM_BP_DIRECT	GO:0006879~cellular iron ion homeostasis	3	5.4	14.4	0.017	0.789	LCN2, HPX, TRF
	GOTERM_CC_DIRECT	GO:0071944~cell periphery	3	5.4	13.2	0.021	0.263	KRT18, KRT8, NID1
	GOTERM_BP_DIRECT	GO:0005604~basement membrane	3	5.4	12.9	0.022	0.252	LAD1, NID1, TRF
	GOTERM_BP_DIRECT	GO:0007160~cell-matrix adhesion	3	5.4	12.4	0.023	0.831	COL3A1, ITGB6, NID1
	GOTERM_BP_DIRECT	GO:0007049~cell cycle	7	12.5	3.1	0.023	0.789	KIF23, CDKN1A, MKI67, NEK3, ANLN, CENPE, HAUS8
	GOTERM_BP_DIRECT	GO:0042060~wound healing	3	5.4	10.9	0.030	0.829	COL3A1, ARHGEF19, COL1A1
	GOTERM_BP_DIRECT	GO:0045095~keratin filament	2	3.6	61.7	0.031	0.318	KRT18, KRT8
	GOTERM_BP_DIRECT	GO:0007229~integrin-mediated signaling pathway	3	5.4	9.9	0.035	0.849	ADAM11, COL3A1, ITGB6
	GOTERM_BP_DIRECT	GO:0035023~regulation of Rho protein signal transduction	3	5.4	9.9	0.035	0.849	ARHGEF1, ARHGEF19, EPS8L2
	GOTERM_BP_DIRECT	GO:0034366~spherical high-density lipoprotein particle	2	3.6	44.1	0.044	0.388	CLU, APOC2
	GOTERM_BP_DIRECT	GO:0018149~peptide cross-linking	2	3.6	42.5	0.045	0.892	COL3A1, TGM2
	GOTERM_BP_DIRECT	GO:0098586~cellular response to virus	2	3.6	42.5	0.045	0.892	IKBKE, FLT3
	GOTERM_BP_DIRECT	GO:0071356~cellular response to tumor necrosis factor	3	5.4	8.6	0.046	0.873	LCN2, CCL2, COL1A1
	GOTERM_BP_DIRECT	GO:0051301~cell division	5	8.9	3.6	0.047	0.861	KIF23, NEK3, ANLN, CENPE, HAUS8
Repressed	GOTERM_BP_DIRECT	GO:0045834~positive regulation of lipid metabolic process	7	9.3	60.7	5.75E-10	1.91E-07	MUP1, MUP3, MUP2, MUP18, MUP9, ANGPTL4, MUP11
	GOTERM_BP_DIRECT	GO:0031649~heat generation	6	8.0	56.4	3.29E-08	5.46E-06	MUP1, MUP3, MUP2, MUP18, MUP9, MUP11
	GOTERM_BP_DIRECT	GO:0071396~cellular response to lipid	6	8.0	56.4	3.29E-08	5.46E-06	MUP1, MUP3, MUP2, MUP18, MUP9, MUP11
	GOTERM_BP_DIRECT	GO:0051055~negative regulation of lipid biosynthetic process	6	8.0	52.0	5.31E-08	5.88E-06	MUP1, MUP3, MUP2, MUP18, MUP9, MUP11
	GOTERM_BP_DIRECT	GO:0006112~energy reserve metabolic process	6	8.0	45.1	1.22E-07	1.01E-05	MUP1, MUP3, MUP2, MUP18, MUP9, MUP11
	GOTERM_BP_DIRECT	GO:0010888~negative regulation of lipid storage	6	8.0	42.3	1.77E-07	1.17E-05	MUP1, MUP3, MUP2, MUP18, MUP9, MUP11
	GOTERM_BP_DIRECT	GO:0045721~negative regulation of gluconeogenesis	6	8.0	42.3	1.77E-07	1.17E-05	MUP1, MUP3, MUP2, MUP18, MUP9, MUP11
	GOTERM_BP_DIRECT	GO:0045475~locomotor rhythm	6	8.0	39.8	2.48E-07	1.37E-05	MUP1, MUP3, MUP2, MUP18, MUP9, MUP11
	GOTERM_BP_DIRECT	GO:0061179~negative regulation of insulin secretion involved in cellular response to glucose stimu	6	8.0	39.8	2.48E-07	1.37E-05	MUP1, MUP3, MUP2, MUP18, MUP9, MUP11
	GOTERM_BP_DIRECT	GO:0010907~positive regulation of glucose metabolic process	6	8.0	37.6	3.42E-07	1.62E-05	MUP1, MUP3, MUP2, MUP18, MUP9, MUP11
	GOTERM_BP_DIRECT	GO:0070584~mitochondrion morphogenesis	6	8.0	25.1	3.03E-06	1.26E-04	MUP1, MUP3, MUP2, MUP18, MUP9, MUP11
	GOTERM_BP_DIRECT	GO:0051897~positive regulation of protein kinase B signaling	7	9.3	15.2	5.23E-06	1.93E-04	MUP1, MUP3, MUP2, MUP18, CPNE1, MUP9, MUP11
	GOTERM_BP_DIRECT	GO:0009060~aerobic respiration	6	8.0	20.5	8.56E-06	2.84E-04	MUP1, MUP3, MUP2, MUP18, MUP9, MUP11
	KEGG_PATHWAY	mmu03320:PPAR signaling pathway	7	9.3	12.9	1.02E-05	6.33E-04	CYP4A10, ACOX1, EHHADH, FABP1, ACAA1B, SLC27A2, ANGPTL4
	GOTERM_BP_DIRECT	GO:0042593~glucose homeostasis	7	9.3	10.7	4.09E-05	1.23E-03	G6PC, MUP1, MUP3, MUP2, MUP18, MUP9, MUP11
	KEGG_PATHWAY	mmu00830:Retinol metabolism	7	9.3	10.0	4.45E-05	1.38E-03	CYP4A10, UGT1A10, CYP2B9, UGT2B1, CYP3A41A, CYP2C40, RETSAT
	GOTERM_CC_DIRECT	GO:0005576~extracellular region	15	20.0	3.6	4.47E-05	2.86E-03	MUP7, MUP1, MUP3, MUP2, SERPINA1E, MUP10, SERPINA6, PDGFRL, MUP18, MUP17, MUP15, MUP14, MUP9, MUP11, ANGPTL4
	KEGG_PATHWAY	mmu01100:Metabolic pathways	21	28.0	2.4	4.74E-05	9.79E-04	ETNPPL, ACOX1, CYP2J9, GNE, EHHADH, CYP2B9, UGT2B1, CYP2C40, UPP2, AK4, LPIN2, LPIN1, CYP4A10, UGT1A10, TDO2, G6PC, HYKK, HMGCS2, HDC, CYP3A41A, ACAA1B
	GOTERM_BP_DIRECT	GO:0071394~cellular response to testosterone stimulus	4	5.3	41.0	9.99E-05	2.76E-03	MUP1, UGT2B1, MUP18, MUP11
	GOTERM_BP_DIRECT	GO:0006635~fatty acid beta-oxidation	5	6.7	16.1	2.27E-04	0.006	ACOX1, ECI2, EHHADH, ACAA1B, SLC27A2
	GOTERM_BP_DIRECT	GO:0035634~response to stilbenoid	4	5.3	22.5	6.53E-04	0.015	SLCO1A1, MUP1, MUP3, CYP2B9
	KEGG_PATHWAY	mmu00071:Fatty acid degradation	5	6.7	11.6	7.15E-04	0.011	CYP4A10, ACOX1, ECI2, EHHADH, ACAA1B
	GOTERM_CC_DIRECT	GO:0005829~cytosol	21	28.0	2.1	9.16E-04	0.029	TXNIP, MUP1, GNE, MUP3, EHHADH, MUP2, LPIN2, GPCPD1, INMT, STARD4, ULK1, HDC, CPNE1, CES1F, MUP18, GYS2, FABP1, YOD1, MUP9, CAR3, MUP11
	GOTERM_BP_DIRECT	GO:0009062~fatty acid catabolic process	3	4.0	42.3	2.03E-03	0.044	ECI2, LPIN2, LPIN1
	KEGG_PATHWAY	mmu00140:Steroid hormone biosynthesis	5	6.7	8.5	2.29E-03	0.028	UGT1A10, CYP2B9, UGT2B1, CYP3A41A, CYP2C40
	GOTERM_BP_DIRECT	GO:0008152~metabolic process	9	12.0	3.7	2.33E-03	0.047	UGT1A10, ACOX1, ECI2, HMGCS2, GNE, EHHADH, GYS2, ACAA1B, SLC27A2
	GOTERM_BP_DIRECT	GO:0006631~fatty acid metabolic process	6	8.0	6.2	2.53E-03	0.048	CYP4A10, ACOX1, EHHADH, LPIN2, ACAA1B, SLC27A2
	GOTERM_BP_DIRECT	GO:0043252~sodium-independent organic anion transport	3	4.0	37.6	2.60E-03	0.047	SLCO1B2, SLCO1A1, SLC22A26
	GOTERM_BP_DIRECT	GO:0006629~lipid metabolic process	9	12.0	3.6	3.04E-03	0.052	ACOX1, HMGCS2, EHHADH, ASPG, LPIN2, GPCPD1, ACAA1B, SLC27A2, LPIN1
	GOTERM_BP_DIRECT	GO:0045892~negative regulation of transcription, DNA-templated	9	12.0	3.5	3.46E-03	0.056	MUP1, NR1D2, KLF10, MUP3, MUP2, MUP18, BCL6, MUP9, MUP11
	GOTERM_BP_DIRECT	GO:0005789~endoplasmic reticulum membrane	11	14.7	2.9	3.91E-03	0.080	CYP4A10, LRIT1, F830016B08RIK, CYP2B9, CYP3A41A, CYP2C40, LPIN2, GM4951, SLC27A2, LPIN1, RETSAT
	KEGG_PATHWAY	mmu05204:Chemical carcinogenesis	5	6.7	7.0	0.005	0.049	UGT1A10, CYP2B9, UGT2B1, CYP3A41A, CYP2C40
	KEGG_PATHWAY	mmu04146:Peroxisome	5	6.7	6.3	0.007	0.060	ACOX1, ECI2, EHHADH, ACAA1B, SLC27A2
	KEGG_PATHWAY	mmu00590:Arachidonic acid metabolism	4	5.3	9.5	0.007	0.057	CYP4A10, CYP2J9, CYP2B9, CYP2C40
	GOTERM_BP_DIRECT	GO:0005777~peroxisome	5	6.7	5.5	0.012	0.180	ACOX1, ECI2, EHHADH, ACAA1B, SLC27A2
	GOTERM_BP_DIRECT	GO:0055114~oxidation-reduction process	10	13.3	2.6	0.013	0.192	CYP4A10, ACOX1, TDO2, EHHADH, CYP2B9, CYP3A41A, CYP2C40, SDR9C7, AKR1C14, RETSAT
	GOTERM_BP_DIRECT	GO:0019373~epoxygenase P450 pathway	3	4.0	16.1	0.014	0.194	CYP2C69, CYP2B9, CYP2C40
	GOTERM_CC_DIRECT	GO:0031090~organelle membrane	4	5.3	7.4	0.016	0.189	CYP4A10, CYP2B9, CYP3A41A, CYP2C40
	GOTERM_CC_DIRECT	GO:0005783~endoplasmic reticulum	14	18.7	2.0	0.019	0.183	LRIT1, CYP2J9, CYP2B9, CYP2C40, SERPINA1E, LPIN2, LPIN1, CYP4A10, UGT1A10, G6PC, STARD4, CES1F, SLC27A2, RETSAT
	KEGG_PATHWAY	mmu00564:Glycerophospholipid metabolism	4	5.3	6.6	0.021	0.133	ETNPPL, LPIN2, GPCPD1, LPIN1
	GOTERM_BP_DIRECT	GO:0005887~integral component of plasma membrane	7	9.3	3.1	0.022	0.184	SLCO1B2, SLCO1A1, SLC38A2, SLC22A26, SLC7A2, SLC17A2, SLC22A5
	GOTERM_BP_DIRECT	GO:0010628~positive regulation of gene expression	6	8.0	3.7	0.022	0.278	MUP1, MUP3, MUP2, MUP18, MUP9, MUP11
	KEGG_PATHWAY	mmu00591:Linoleic acid metabolism	3	4.0	11.8	0.025	0.144	CYP2J9, CYP3A41A, CYP2C40
	GOTERM_BP_DIRECT	GO:0055088~lipid homeostasis	3	4.0	11.7	0.026	0.308	ACOX1, G6PC, NR1D2
	GOTERM_CC_DIRECT	GO:0005615~extracellular space	10	13.3	2.3	0.027	0.197	MUP1, SERPINA6, MUP3, MUP2, MUP18, CES1F, SERPINA1E, MUP9, ANGPTL4, MUP11
	GOTERM_BP_DIRECT	GO:1901223~negative regulation of NIK/NF-kappaB signaling	2	2.7	56.4	0.034	0.373	NLRP12, CPNE1
	GOTERM_BP_DIRECT	GO:0006814~sodium ion transport	3	4.0	9.7	0.037	0.383	SLC38A2, SLC17A2, SLC22A5
	KEGG_PATHWAY	mmu00380:Tryptophan metabolism	3	4.0	9.0	0.041	0.208	TDO2, EHHADH, INMT
	GOTERM_BP_DIRECT	GO:0007610~behavior	2	2.7	45.1	0.043	0.417	MUP18, MUP11
	GOTERM_BP_DIRECT	GO:0050727~regulation of inflammatory response	3	4.0	8.9	0.043	0.408	NR1D2, SLC7A2, BCL6

Supplementary Table 2: Enriched GO terms and corresponding genes from RNA sequencing performed on microdissected (xMD) BECs

Gene symbol	Accession number	Forward	Reverse
18S	NM_003278	5' - AACTTTCgATggTAgTCgCCgT - 3'	5' - TCCTTggATgTggTAgCCgTTT - 3'
Acta2	NM_007392.3	5' - AACAgCATCATgAAgTgTgATATTgACATC - 3'	5' - gCTgATCCACATCTgCTggAAgg - 3'
Afp	NM_007423.4	5' - TgACAACAAggAggAgTgCTTCCA - 3'	5' - AATggTTgTTgCCTggAggTTTCg - 3'
Angpt2	NM_007426.4	5' - AgCCCCTACATgTCCAATgC - 3'	5' - TTgTgCTgCTgTCTggTTCA - 3'
Ccl2	NM_011333.3	5' - TCTGGACCCATTCCTTCTTGG - 3'	5' - TCAGCCAGATGCAGTTAACGC - 3'
Cd133	NM_008935.2	5' - CCCTCCAgCAAACAAgCAAC - 3'	5' - ACAgCCggAAgTAAgAgCAC - 3'
Col1a1	NM_007742	5' - gAAACCgCAggTATgCTTgA - 3'	5' - gACCAggAggACCAggAAgT - 3'
Col3a1	NM_009930.2	5' - TAggACTgACCAAggTggCT - 3'	5' - ggAACCTggTTTCTTCTCACC - 3'
Col5a2	NM_007737.2	5' - CATggAgAAggTTTCCAAATg - 3'	5' - AAAgCCCAggAACAAgAgAA - 3'
Cyp7a1	NM_007824.2	5' - ATTCCATACCTgggCTgTgC - 3'	5' - CTgTgTCCAAATgCCTTCgC - 3'
Cyp8b1	NM_010012.3	5' - TCCTCAgggTggTACAggAg - 3'	5' - CgggTTgAggAACCgATCAT - 3'
Eln	NM_007925.4	5' - ATAAAACgAggCgCTgAgAg - 3'	5' - CTCCAggACCTgCTCCAAAC - 3'
Entpd2	NM_009849.2	5' - ATgCgCCTACTCAACCTgAC - 3'	5' - AgCAggTAgTTggCAgTCAC - 3'
Fxr	NM_001163700.1	5' - ggCTgCAAAggTTTCTTCCg - 3'	5' - ACACTggATTTCAgTTAACAAACC - 3'
Fn1	NM_010233.2	5' - gACCCTTACACggTTTCCCA - 3'	5' - ACgTTgCTTCATggggATCA - 3'
Gpbar1 (TGR5)	NM_174985.1	5' - CgATgTACCCTCAACCCTgg - 3'	5' - ACgCTCATAggCCAAgACTg - 3'
Hif1a	NM_001313919.1	5' - TggACTTgTCTCTTTCTCCgC - 3'	5' - TTTTCTTCTCgTTCTCgCCg - 3'
Il1b	NM_008361	5' - CTCCACCTCAATggACAgAA - 3'	5' - gCCgTCTTTCATTACACAgg - 3'
Il6	NM_013693	5' - gAACAACgATgATgCACTTgC - 3'	5' - TCCAggTAgCTATggTACTCC - 3'
Ifng	NM_008337	5' - ggCCATCAgCAACAACATAAgCgT - 3'	5' - TgggTTgTTgACCTCAAACTTggC - 3'
Itgb1	NM_010578.2	5' - ggACgCTgCgAAAAgATgAA - 3'	5' - CCACAATTTggCCCTgCTTg - 3'
Itgb5	NM_001145884.1	5' - gCCCgTTATgAAATggCCTC - 3'	5' - CTACCAggTCCCTTAgggCT - 3'
Itgb6	NM_021359.3	5' - ACggCTTCCAgCTTTggTC - 3'	5' - ACAggTgggTgAAATTCTCCTg - 3'
Itgb8	NM_177290.3	5' - ACTgggCCAAAgTgAACACA - 3'	5' - ACTgAgACTTCTCCCggTgT - 3'
Lta	NM_010735.2	5' - AgCAgCATCTTCTAAgCCCT - 3'	5' - gTCATgTggAgAACCTgCTgTg - 3'
Ltb	NM_008518.2	5' - CAgCTgCggATTCTACACCA - 3'	5' - CATCCAAgCgCCTATgAggT - 3'
Osm	NM_001013365.2	5' - gAgCCCTATATCCgCCTCCA - 3'	5' - AgCTTTggAAAAgCCggAGT - 3'
Pkm2	NM_001253883.1	5' - CCCgCAACACTggCATCATTTgTA - 3'	5' - TgCAAAgCTTTCTgTggCTTCACg - 3'
Tgfb1	NM_011577	5' - TgCgCTTgCAgAgATTAAAA - 3'	5' - CTgCCgTACAACTCCAgTgA - 3'
Tgfb2	NM_009367.3	5' - TCCCCTCCgAAAATgCCATC - 3'	5' - TgCTATCgATgTAgCgCTgg - 3'
Thy1	NM_009382.3	5' - AACCAAAACCTTCgCCTggAC - 3'	5' - AAgCTCACAAAAgTAgTCgCCC - 3'
Tnfa	NM_013693	5' - AATggCCTCCCTCTCATCAgTT - 3'	5' - CCACTTggTggTTTgCTACgA - 3'
Tweak (Tnfsf12)	NM_011614.3	5' - AATCAACAgCTCCAgCCCTC - 3'	5' - gATCCgAAgggAAgACCCTg - 3'

Supplementary Table 3: Oligonucleotides used for quantitative RT-PCR